

Quasi-zero-stiffness vibration isolation: Designs, improvements and applications



Chaoran Liu^{a,*}, Wei Zhang^{a,b,**}, Kaiping Yu^c, Tao Liu^a, Yan Zheng^d

^a Beijing Key Laboratory on Nonlinear Vibrations and Strength of Mechanical Structures, Beijing University of Technology, Beijing 100124, China

^b Department of Mechanics, Guangxi University, Nanning 530004, China

^c Department of Astronautic Science and Mechanics, Harbin Institute of Technology, Harbin 150001, China

^d Department of Mathematics, Beijing Institute of Graphic Communication, Beijing 102600, China

ARTICLE INFO

Keywords:

Quasi-zero-stiffness
Nonlinear vibration isolation
Improvement strategies

ABSTRACT

Most of the engineering vibrations are harmful, due to many unfavorable consequences caused by them, such as structural damage, poor working accuracy, etc., making it necessary to implement vibration isolation measures. Traditional linear vibration isolation methods have significant deficiencies regarding isolating low-frequency vibrations, in which the stiffness of the isolation system becomes a dominant factor. The quasi-zero-stiffness (QZS) vibration isolation technology, developed in recent decades, can greatly reduce the dynamic stiffness without reducing the static stiffness and thus extend the vibration isolation frequency band to low frequency region. A variety of approaches for constructing QZS isolators have been proposed based on geometric nonlinearity, magnetic nonlinearity, deformable components and so on. With higher demands and more complex operating conditions, many improvement strategies have been proposed to further enhance the overall performance of QZS isolators from various aspects. To date, a small portion of theoretical achievements in QZS vibration isolation have been applied in engineering fields, showing great advantages over linear vibration isolation methods. In these contexts, a comprehensive review of the QZS vibration isolation technology is essential. This paper is devoted to summarize the main research progress of QZS vibration isolation in terms of designs, improvement strategies and applications, to provide a general overview of the QZS vibration isolation technology for researchers in related fields.

1. Introduction

Vibration is a ubiquitous phenomenon in the natural world and engineering fields, which might sometimes be exploited to achieve specific purposes in a few cases, but the vast majority of vibrations in engineering are harmful since they can cause many undesirable consequences. For example, the vibrations of the optical payloads in remote sensing satellites severely restrict the imaging resolutions, the vibrations of vehicle seats reduce ride comfort, and the vibrations of machine tools reduce the machining precision. In civil engineering, metro-induced vertical vibrations and vibration-induced noises generally cause discomfort to occupants in adjacent buildings [1], and earthquake-induced vibrations often lead to the damage of buildings and large civil structures [2]. Therefore, there is an urgent need for a

methodology for suppressing vibrations in engineering [3]. In mechanical engineering and aerospace engineering, the most common method of vibration suppression is vibration isolation, which refers to the use of an additional system between the vibration source and the controlled object to isolate the vibration transmitted from the former to the latter, thereby achieving the purpose of vibration suppression of the controlled object. In civil engineering, there are also several other alternatives for vibration suppression, such as the active and semi-active structural vibration control via smart materials [4], tuned mass damper [5], etc. The essence of vibration isolation is to hamper the mechanical energy transmission from the vibration source to the controlled object, thus reducing the vibration of the controlled object. The earliest passive vibration isolation method is the linear isolator, which can be modelled as a spring-mass-damper system. The effective

* Corresponding author.

** Corresponding author at: Beijing Key Laboratory on Nonlinear Vibrations and Strength of Mechanical Structures, Beijing University of Technology, Beijing 100124, China

E-mail addresses: chaoran@bjut.edu.cn (C. Liu), sandyzhang9@163.com (W. Zhang).

vibration isolation frequency band of the linear isolator starts from $\sqrt{2}$ times the natural frequency [6]. To extend the vibration isolation frequency band to lower frequency region, the natural frequency must be reduced. For a definite isolation object, the only way to reduce the natural frequency is to reduce the stiffness, but too low a stiffness will weaken the load bearing capacity. Therefore, there is an inevitable contradiction between the vibration isolation frequency band and the load bearing capacity for a linear vibration isolator, rendering it unsuitable for low-frequency vibration isolation.

In order to resolve the drawback of linear vibration isolators, nonlinear vibration isolation methodologies [7] were proposed in recent decades, of which the most representative is the quasi-zero-stiffness (QZS) vibration isolation technology. Unlike linear isolators, which do not distinguish between dynamic stiffness and static stiffness, QZS isolators exhibit disparate stiffness characteristics. The dynamic stiffness, defined as the derivative of restoring force with respect to displacement, can be intentionally designed to be very small or even zero in the vicinity of the static equilibrium point. In contrast, the static stiffness, which refers to the ratio between the restoring force at the static equilibrium position and the displacement from the initial position to the static equilibrium position, can be designed to be very large. This nonlinear characteristic of low dynamic stiffness and high static stiffness can greatly reduce the "natural frequency" of the system while maintaining a high load bearing capacity, thereby extending the vibration isolation frequency band to low frequency region. The general principle for achieving the QZS property is to connect the positive stiffness element and the negative stiffness element in parallel with well-chosen system parameters [8], as shown in Fig. 1, and the key is to design an appropriate negative stiffness mechanism. The positive stiffness element plays the role of not only providing positive stiffness but also bearing the weight of the isolation object, and the negative stiffness element plays the role of counteracting the positive stiffness around the static equilibrium position, thus producing quasi-zero stiffness for the whole system.

Based on the general principle of connecting positive and negative stiffness elements in parallel to achieve the QZS property, a variety of approaches for constructing QZS isolators have been proposed. These approaches can be broadly divided into three main categories: geometric nonlinearity, magnetic nonlinearity, and exploitation of deformable components. Regarding the first category, the negative stiffness is produced by the nonlinear geometric relationship; regarding the second category, the negative stiffness is produced by the nonlinear magnetic coupling; regarding the third category, the negative stiffness is produced by the nonlinearity in large deformation. Although conventional QZS isolators can already realize much better vibration isolation performance than linear isolators, there is still room for further enhancement. Many improvement strategies have been proposed to perfect the QZS isolators, such as broadening the low-stiffness displacement range, introducing nonlinear damping, etc. Due to the huge advantages of QZS isolators, they have been applied in many engineering cases, such as vehicles, hand-held jackhammer, etc., demonstrating satisfactory results.

In this paper, the research progress of QZS vibration isolation

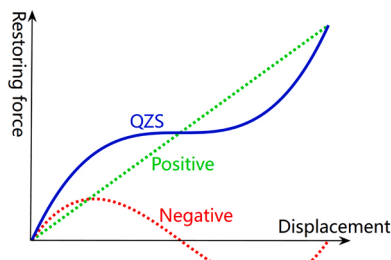


Fig. 1. General principle for achieving QZS property.

technology in recent decades is reviewed in terms of designs, improvements and applications. In Section 2, the approaches for constructing QZS isolators are discussed. In Section 3, multi-degree-of-freedom (MDOF) QZS isolation systems, including one-piece-type MDOF QZS isolators and platform-type 6DOF QZS isolation systems, are briefly introduced. In Section 4, improvement strategies are expounded to further enhance the QZS isolators for superior overall performance. In Section 5, some application examples of the QZS isolators in engineering are presented. In Section 6, this paper is briefly summarized, and some future prospects are provided. The objective of this paper is to provide a comprehensive overview of QZS vibration isolation for researchers in related fields, aiding them in further exploration and development of the QZS vibration isolation technology.

2. Construction approaches for QZS isolators

In general, the key to constructing a QZS isolator is to design a negative stiffness mechanism and then connect it in parallel with a matched positive stiffness element (usually with linear positive stiffness) to achieve quasi-zero dynamic stiffness. (Note that there are also a small number of QZS isolators that are not constructed based on this general principle.) The structural and physical parameters should be properly designed to make the negative stiffness exactly counteract the positive stiffness at the static equilibrium point for the realization of QZS characteristic.

For the vast majority of QZS isolators, the first-order derivative of the restoring force with respect to the displacement is zero at the static equilibrium point. In this regard, the stiffness characteristic of the QZS isolator is similar to that of the nonlinear energy sink (NES) which is actually a purely nonlinear oscillator without linear stiffness [9]. Besides, both of them can be employed for vibration suppression. The essential difference lies in the implementation manner and the location of vibration suppression object. The QZS isolator directly supports the vibration suppression object for the sake of a low resonant frequency, and the essence is vibration "isolation". However, the NES must be attached to a primary system to suppress the vibration of the primary system over a wide frequency range via targeted energy transfer [10], and the essence is vibration "absorption".

2.1. Exploiting geometric nonlinearity

The QZS isolators based on geometric nonlinearity (hereafter called geometrically nonlinear QZS isolators) are composed of the springs that can be treated as ideal spring elements and the 'rigid' components whose elastic deformation can be neglected. In practice, these 'rigid' components (such as linkages, cams, sliders, etc.) have very small deformation that exerts almost no effect on the stiffness characteristics of the whole system, and therefore can be considered rigid in the theoretical analysis. Although the stiffnesses of the springs are generally linear, the continuous variation of the geometric attributes (such as the angle) of the springs or 'rigid' components during vibration causes the total restoring force—displacement relationship to exhibit nonlinear properties [11], and then the whole system can realize QZS characteristic by properly designing the geometric parameters and spring stiffness.

2.1.1. Classic designs

The most widely studied geometrically nonlinear QZS isolator is composed of three springs, as shown in Fig. 2(a) [12], two of which are oblique to provide negative stiffness in the vicinity of the static equilibrium point [13], and the vertical spring provides positive stiffness. The total restoring force—displacement relationship is [14].

$$f_{res}(x) = 2k_o(h_0 - x) \left(\frac{\sqrt{h_0^2 + a^2}}{\sqrt{(h_0 - x)^2 + a^2}} - 1 \right) + k_v x \quad (1)$$

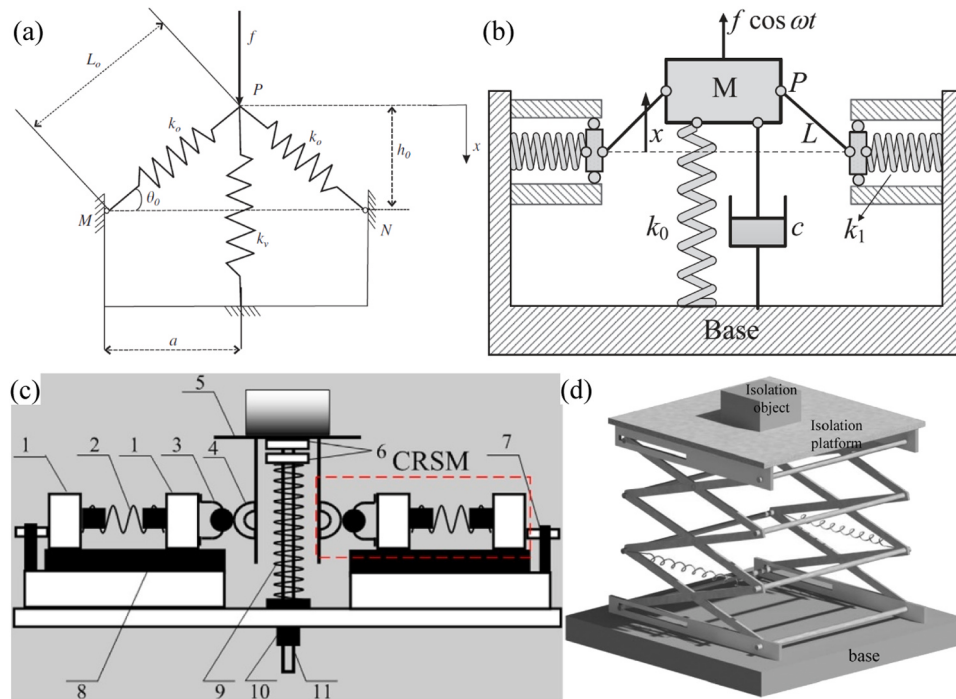


Fig. 2. Classic designs of QZS isolators based on geometric nonlinearity: (a) three-spring QZS isolator; (b) spring-linkage type QZS isolator; (c) cam-roller-spring type QZS isolator; (d) scissor-like QZS isolator.

The parameter condition for realizing QZS is $2k_o/k_v = a/(L_0 - a)$. Zhang et al. [15] studied the bursting oscillation of this kind of QZS isolator; Hao et al. [16] studied some complex nonlinear dynamic phenomena of the three-spring QZS isolator such as local bifurcation, global bifurcation and invariant manifold; Liu et al. [17] established an accurate dynamic model for the three-spring QZS isolator with consideration of the deformation damping and rotation damping of the oblique springs; Lan et al. [18] fabricated a compact prototype using planar springs and tested its isolation performance; Tian et al. [19] studied the vibration isolation performance of a rectangular panel supported by four three-spring QZS isolators; Xu et al. [20] utilized four identical oblique springs and a vertical spring to form a five-spring QZS isolator which is the same as the three-spring QZS isolator in essence but has better stability; Liu et al. [21] used transverse groove springs to fabricate an experimental prototype for the five-spring QZS isolator, whose beginning frequency for vibration isolation is as low as 2.82 Hz.

Another classic example of geometrically nonlinear QZS isolator is the spring-linkage type QZS isolator [22], as shown in Fig. 2(b), in which the two horizontal springs are in the compressed state and the linkages transform the horizontal spring forces into the vertical direction to produce negative stiffness, while the vertical spring provides positive stiffness. The total restoring force–displacement relationship is [23].

$$f_{res}(x) = k_0x - 2k_1x \left(1 - \frac{L-h}{\sqrt{L^2-x^2}}\right) \quad (2)$$

where h is the initial compression of the horizontal spring at the static equilibrium position and the other parameters are provided in Fig. 2(b). The parameter condition for realizing QZS is $k_0L = 2k_1h$. Liu et al. [24] studied the superharmonic resonance of the spring-linkage type and revealed that it will deteriorate the isolation performance at frequencies below the superharmonic truncation frequency, but the beginning frequency for vibration isolation is almost unaffected.

Zhou et al. [25] designed a cam-roller-spring type QZS isolator as shown in Fig. 2(c), in which the forces of the initially compressed horizontal springs are converted into the vertical direction through the cam-roller pairs to produce negative stiffness, and the positive stiffness

is provided by the vertical spring. The total restoring force–displacement relationship for the cam-roller-spring type QZS isolator is

$$f_{res}(x) = \begin{cases} k_v x - 2k_h x \left[1 + \frac{\delta - (r_1 + r_2)}{\sqrt{(r_1 + r_2)^2 - x^2}}\right] & |x| < x_d \\ k_v x |x| & |x| \geq x_d \end{cases} \quad (3)$$

where k_v and k_h are the stiffnesses of the vertical and horizontal springs respectively, r_1 and r_2 are the radii of the roller and cam respectively, and δ is the initial compression of the horizontal spring. Different from the aforementioned two kinds of geometrically nonlinear QZS isolators, the restoring force–displacement relationship of the cam-roller-spring type QZS isolator is a piecewise function, as shown in Fig. 3. For a relatively small displacement, the cam and the corresponding roller remain in contact, possessing nonlinear stiffness, and the QZS characteristic is realized when $2k_h\delta = k_v(r_1 + r_2)$. For a relatively large displacement, the cam and the roller disengage from each other, possessing linear stiffness. Zhou et al. [26] redesigned the cam-roller-spring

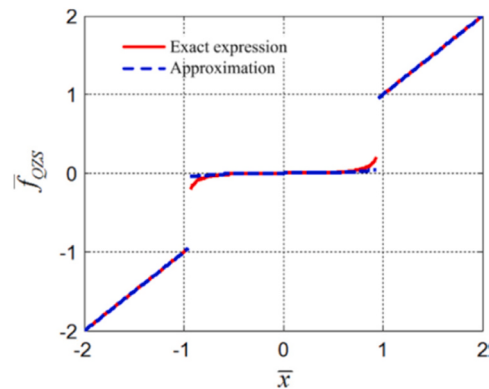


Fig. 3. Dimensionless restoring force–displacement relationship of the cam-roller-spring type QZS isolator.

type QZS isolator for torsional vibration isolation, and Wang et al. [27] studied the effects of parameter errors on the isolation performance of the torsional cam-roller-spring type QZS isolator, revealing that the degradation on the performance caused by a single error can be eliminated by a combination of multiple errors due to a mutual counteraction of these influences.

Sun and Jing [28] proposed a QZS isolator with a scissor-like structure (also called the X-shaped structure [29]), as shown in Fig. 2(d), whose restoring force–displacement relationship is

$$f_{res}(y) = \frac{k}{n} \left(2l \sin \theta - \frac{y}{n} \right) \left[1 - \frac{l \cos \theta}{\sqrt{l^2 - (l \sin \theta - y/2n)^2}} \right] \quad (4)$$

where l is the half length of the linkage, k is the stiffness of the spring, n is the number of layers, and θ is the angle between the linkage and the horizontal direction when the spring is undeformed. From the unloaded position, the restoring force is increased first and then decreased with the displacement, thereby exhibiting positive stiffness first and then negative stiffness. At the critical point between the displacement intervals for positive stiffness and for negative stiffness, the tangent slope of the restoring force to displacement is zero, corresponding to the zero stiffness point. Since the right side of the zero stiffness point is the displacement range for negative stiffness, the static equilibrium point should be designed in the left vicinity of the zero stiffness point rather than the zero stiffness point itself to avoid static instability [30]. In contrast to the aforementioned three kinds of geometrically nonlinear QZS isolators, the design principle of the scissor-like QZS isolator is not the parallel connection of positive and negative stiffness elements, and its restoring force–displacement relationship is asymmetric, which causes the oscillation center not to coincide with the static equilibrium point [31]. The major advantage of the scissor-like QZS isolator is its strong designability and reformability, which can be tailored to practical working conditions, and other elements can be added to the scissor-like structure to enhance the isolation performance [32].

2.1.2. Other designs based on geometric nonlinearity

Han et al. [33] designed a QZS isolator composed of four linkages and two springs based on geometric nonlinearity as shown in Fig. 4(a), in which the horizontal spring and four linkages form the negative stiffness element with two geometric states: bulged-out and nested-in, and the vertical spring provides positive stiffness. The damping in rotational joints was considered in the dynamic modelling process, and the results indicated that rotational damping is beneficial for isolation performance. Similarly, Ye et al. [34] designed a QZS isolator using “rigid” facets and coil springs as shown in Fig. 4(b), in which the horizontal springs and “rigid” facets form the negative stiffness element with two geometric states, convex state and concave state, and the vertical spring provides positive stiffness.

Bio-inspired QZS vibration isolators are mainly based on geometric nonlinearity. The classic scissor-like QZS isolator (X-shaped QZS isolator) enhanced by nonlinear inertia coupling can actually be seen as a bio-inspired structure mimicking the human body [35]. Zeng et al. [36] designed a geometrically nonlinear QZS isolator using torsional springs and linkages as shown in Fig. 4(c), which was inspired by the M-like limbs of frogs. Ling et al. [37] designed a QZS structure mimicking the body topology of the cockroach for low-frequency vibration isolation, as shown in Fig. 4(d), which can withstand forces up to 900 times the body weight owing to the shape-changing ability of their jointed exoskeletons and striated muscles. The exoskeletons, striated muscles and front legs were mimicked by a diamond-shape chamber, springs, and rods with sliders, respectively. The diamond-shape chamber contributes to nonlinear low dynamic stiffness and the sliders lead to nonlinear damping and inertia effects. They also designed a click-beetle-inspired QZS structure [38] for ultralow frequency vibration isolation as shown in Fig. 4(e). The proposed structure possesses three postures: the unbending posture, the down-bending posture and the up-bending posture. Based on these three postures, the stiffness can be tuned easily among negative, quasi-zero, zero and small positive by adjustment of the initial assembly angle, length ratio and linear stiffness ratio. The QZS region can be designed to be extremely large under some special parameters, so as to broaden the effective working range.

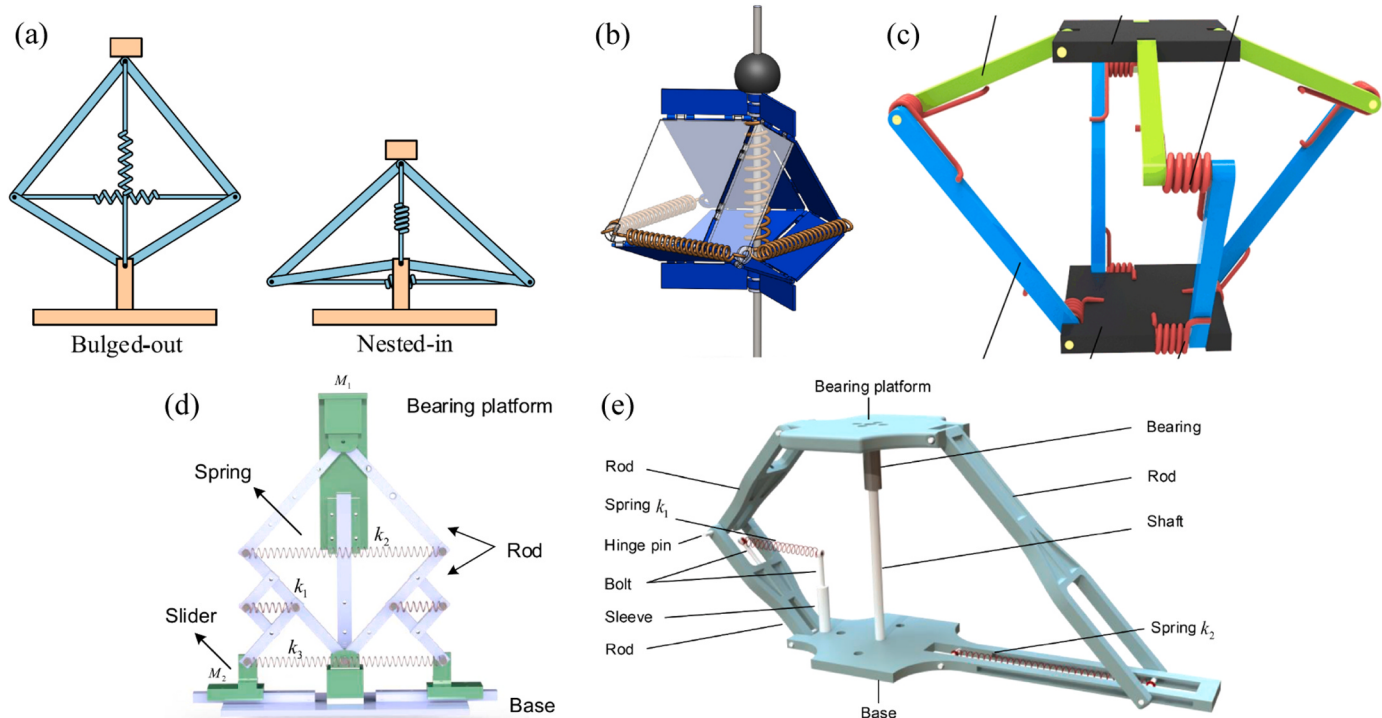


Fig. 4. QZS isolators based on geometric nonlinearity: (a) using springs and linkages; (b) using springs and facets; (c) inspired by limbs of frog; (d) inspired by cockroach; (e) inspired by click beetle.

The combination of geometric nonlinearity and gravity effect contributes to the development of the track NES (T-NES) [39]. The restoring force of the track NES is produced by the horizontal component of the normal force between the track and the NES mass due to gravity. Therefore, by designing the profile of the track properly, various stiffness characteristics can be obtained, indicating strong designability. The fourth-order polynomial is often used as the profile function of the track [40], which results in a restoring force in the purely third-order polynomial form.

2.2. Exploiting deformable components

Many flexible components are able to exhibit nonlinear characteristics when experiencing large deformation, which can thus be properly configured to produce negative stiffness in a certain direction, making them candidates for constructing QZS isolators.

2.2.1. Using beams

Buckled beams have been widely employed to produce negative stiffness in the design of QZS isolators. A buckled beam hinged at both ends exhibits softening positive stiffness in its axial direction within a certain displacement range, whose force—displacement relation is [41].

$$P = P_e \left[1 - \frac{\pi q_0}{L} \left(\frac{\pi^2 q_0^2}{L^2} + \frac{4y}{L} \right)^{-1/2} \right] \left(1 + \frac{\pi^2 q_0^2}{8L^2} + \frac{y}{2L} \right) \quad (5)$$

where $P_e = EI(\pi/L)^2$ is the critical buckling load of a hinged beam. Liu et al. [42] replaced the oblique springs in the three-spring QZS isolator with the buckled beams to form a buckled-beam-based QZS isolator, as shown in Fig. 5(a). The restoring force—displacement relationship of this isolator is

$$f_{res}(x) = P_e \left[1 - \frac{\pi q_0}{L} \left(\frac{\pi^2 q_0^2}{L^2} + 4 - 4 \sqrt{\left(\sqrt{1 - \frac{a^2}{L^2}} - \frac{x}{L} \right)^2 + \frac{a^2}{L^2}} \right)^{-1/2} \right] \\ \cdot \left[3 + \frac{\pi^2 q_0^2}{4L^2} - \sqrt{\left(\sqrt{1 - \frac{a^2}{L^2}} - \frac{x}{L} \right)^2 + \frac{a^2}{L^2}} \right] \frac{\sqrt{L^2 - a^2} - x}{\sqrt{(\sqrt{L^2 - a^2} - x)^2 + a^2}} + kx \quad (6)$$

Since the relationship given in Eq.(6) is relatively complicated, Huang et al. [43] approximated it with a third-order polynomial to simplify the theoretical analysis, and studied the effects of system imperfections (including stiffness imperfection, load imperfection and excitation imperfection) on the dynamic characteristics and isolation performance, revealing that the dynamic response will exhibit softening, hardening, and softening-to-hardening characteristics, depending on the combined effect of load imperfection, stiffness imperfection, and excitation amplitude [44]. Chen et al. [45] added an adjustable slider at one end of the buckled beam to tune its static compression, so as to regulate the stiffness characteristics of the whole system. Liu et al. [46] attached

piezoelectric layers on the buckled beams for both low-frequency vibration isolation and energy harvesting. Zhang et al. [47] utilized the buckled beams as negative stiffness element and the folded beams as positive stiffness element to design a compliant QZS isolator with a compact and lightweight structure for low-frequency torsional vibration isolation in the shaft system.

The aforementioned buckled-beam-based QZS isolators consist of the buckled beams with hinged boundary conditions, while those with fixed boundary conditions have also been employed to construct QZS isolators due to the merit of avoidance of friction in revolution joint. Fulcher et al. [48] studied the shock isolation performance of a buckled-beam-based QZS isolator in which the buckled beam is clamped at both ends; the experimental prototype successfully reduced 7 g peak acceleration of the input shock to 1 g peak acceleration of the vibration isolation object. Lian et al. [49] designed the shape of a beam in buckled state to directly produce QZS characteristic and used it as a micro-vibration absorber for low-frequency vibration absorption. Kocak et al. [50] utilized the buckled beams with fixed boundary conditions and two vertical flexure hinges for the design of a compliant lever-type QZS isolator; in this case, the buckled beams provide negative stiffness, while the vertical flexure hinges not only provide positive stiffness but also enable the rotation of the lever arm for inertial amplification to further lower the resonant frequency. Dalela et al. [51] designed a buckled-beam-based QZS isolator consisting of four QZS unit cells with parallel arrangement; in this design, each QZS unit cell is composed of two cosine-shaped beams with fixed boundary conditions and two semicircular arches, as shown in Fig. 5(b); the former possesses negative stiffness due to the buckling-induced snap-through behavior when compressed vertically at the midpoint, and the latter possesses positive stiffness due to the bending-dominated behavior. The QZS unit cell composed of buckled beams and bending-dominated beams can also be exploited to design QZS metamaterials for low-frequency band gap, which was studied by Cai et al. [52] and Fan et al. [53] focusing on one-dimensional and two-dimensional QZS metamaterials respectively.

Huang et al. [54] used sliding beam (also called Gospodnetic-Frisch-Fay beam [55]) to construct a QZS isolator as shown in Fig. 5(c). The sliding beam is placed on two knife-edge supports, which can produce negative stiffness when experiencing large deformation. The restoring force—displacement relationship of the whole isolator is

$$f_{res}(y) = \frac{EI}{l^2} \sum_{n=1}^6 a_{2n-1} \left(\frac{y}{l} \right)^{2n-1} + ky \quad (7)$$

where E is the Young's modulus, I is the inertial moment of cross section, l is the distance between the two supports, a_{2n-1} ($n = 1 \sim 6$) is constant [56] ($a_1 = 48, a_3 = -402, a_5 = 1670.6, a_7 = -3749, a_9 = 4256.4, a_{11} = -1903.5$) and k is the stiffness of the vertical spring. The sliding-beam-based QZS isolator can exhibit softening-to-hardening characteristics, causing the double jump phenomenon to occur in the frequency sweeping process. Qi et al. [57] also utilized the sliding beam to design a QZS isolator, and the difference from Ref.[54] is that the

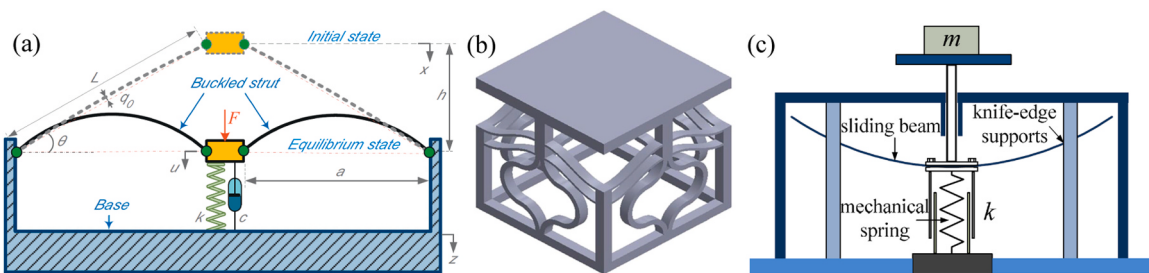


Fig. 5. QZS isolators using beams: (a) using buckled beams with hinged boundary conditions; (b) using buckled beams with fixed boundary conditions; (c) using sliding beam.

repulsive magnets were used as positive stiffness element.

2.2.2. Using composite laminates

Bi-stable composite laminate is generally obtained from multiple layers of fiber reinforced materials by proper stacking design. The stacking sequence is asymmetric about the mid-plane of the plate, and when the plate cools from the curing temperature to room temperature, the directional thermal expansion between the layers allows the plate to warp in two states [58], thus producing two stable equilibrium points, as shown in Fig. 6(a,b). Between the two stable equilibrium points there is an unstable equilibrium point, as shown in Fig. 6(c), in the vicinity of which the stiffness of the plate is negative, so the negative stiffness of the bi-stable plate can be exploited to design the QZS isolator. Shaw et al. [59] connected a carbon fiber reinforced bi-stable laminate and a linear spring in parallel to build a QZS isolator as shown in Fig. 6(d), in which the stacking sequence of the laminate is $[0^\circ \text{ } 3CF, 0^\circ \text{ } 1S, 90^\circ \text{ } 3CF]$. According to the quasi-static test results, the force-displacement relationship of the bi-stable laminate is fitted in the form of $F(z) = Az - B \text{arctan}(Cz)$, and then the restoring force-displacement relationship of the whole isolator is approximated as fifth-order polynomial with only odd terms. Li et al. [60] built a QZS isolator using a bi-stable hybrid symmetric laminate (BSHSL) and a coil spring, in which the BSHSL was formed by stacking aluminum and carbon fiber reinforced polymer (CFRP), and the bi-stability was induced by the thermal expansion mismatch between the CFRP and aluminum in the cooling stage from cure-temperature to room-temperature. The results showed that increasing the length and decreasing the width can improve the isolation performance, while the isolation performance exhibits a nonlinear relationship with the hybrid width; besides, the isolation frequency and peak transmissibility are increased with an increasing number of BSHSLs.

2.2.3. Using origami structures

Origami is the process of folding a finite two-dimensional plane into a three-dimensional complex structure. A variety of spatial structures with nonlinear characteristics can be constructed by designing creases and folding manners. Due to the advantages of the designability and flexibility of origami structures, some researchers have used them to design QZS isolators in recent years. Liu et al. [61,62] designed the geometrical parameters of the Tachi-Miura origami structure as shown in Fig. 7(a) to produce bi-stability, which manifested negative stiffness at the unstable equilibrium point, and then connected it in parallel with a linear positive stiffness spring to achieve QZS characteristic. Sadeghi et al. [63] pumped fluid into the interior of the Miura origami structure and pressurized it, as shown in Fig. 7(b), to obtain asymmetric QZS property through the nonlinear fluid-structure coupling effect as the structural state and internal volume fluctuated. Ishida et al. [64,65] constructed a bi-stable structure using trusses and ball hinges (as shown in Fig. 7(c)), which is similar to Kresling origami in the torsional buckling pattern, and then connected it in parallel with a linear spring to obtain QZS property. The most important feature of the Kresling origami structure is its expandability and contractability. Han et al. [66] made use of this feature to connect several QZS Kresling origamis in parallel to

obtain a lightweight QZS isolator, as shown in Fig. 7(d), and its deployable property makes it suitable for application in aerospace engineering.

2.3. Exploiting magnetic nonlinearity

The magnetic force between magnets is a nonlinear function of displacement and angle. By designing the shape, geometric parameters, relative position, and magnetization direction, the tangent slope of the magnetic restoring force to the displacement can be made negative in a certain displacement range (i.e., the magnetic negative stiffness can be generated). Then it can be connected in parallel with a suitable positive stiffness element to achieve QZS property. The key to designing magnetic QZS isolators lies in the shapes, magnetization directions, and arrangements of the magnets.

2.3.1. Using the simple inverse square law

Xu et al. [67] and Su et al. [68] replaced the horizontal springs of the spring-linkage QZS isolator with two pairs of magnets to obtain a magnetic QZS isolator as shown in Fig. 8(a). Jiang et al. [69] utilized electromagnets instead of permanent magnets to replace the horizontal springs of the spring-linkage QZS isolator, while the positive stiffness was provided by a pneumatic spring, thereby obtaining a magnetic-air hybrid QZS isolator. Zhou et al. [70] designed a QZS isolator using two electromagnets, a permanent magnet, and a beam, as shown in Fig. 8(b), in which the permanent magnet is installed at the middle of the beam providing positive stiffness. Furthermore, the permanent magnet is also arranged between the two electromagnets separated by a certain distance to generate magnetic negative stiffness by adjusting the current direction so that the polarities of the permanent magnet and each electromagnet are opposite (i.e., the two electromagnets are both attractive to the permanent magnet). In the modeling and design process of the aforementioned magnetic QZS isolators, the magnetic force acting between two magnets was taken as

$$F_{\text{magnet}} = \pm \frac{C_m}{d^2} \quad (8)$$

where C_m is a magnetic constant [71] and d represents the distance between the two magnets. Since the magnetic force between two magnets was roughly described in the form of the inverse square of the distance (inverse square law), the effect of the magnet shape on the magnetic force was not considered, and therefore the overall stiffness characteristics were mainly determined by the arrangements and polarities of the magnets.

2.3.2. Using cuboid-shaped magnets

More researchers take into account the shapes of magnets when designing magnetic QZS isolators. The most commonly used magnet shapes are cuboid shape and ring shape. Robertson et al. [72] analytically modeled the interaction force between two cuboid-shaped magnets placed in parallel and with the same direction of magnetization (not necessarily the same polarity) and found that the ratio between the

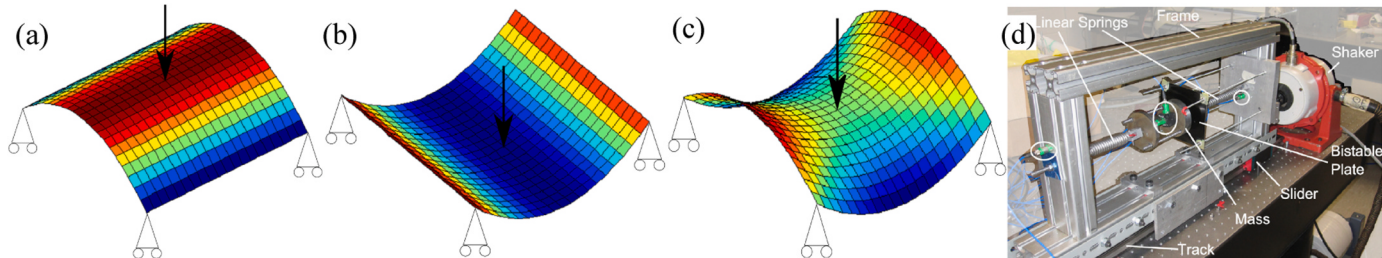


Fig. 6. Bi-stable laminate and the QZS isolator based on bi-stable laminate: (a) the first stable state; (b) the second stable state; (c) the unstable equilibrium stable; (d) the QZS isolator based on bi-stable laminate.

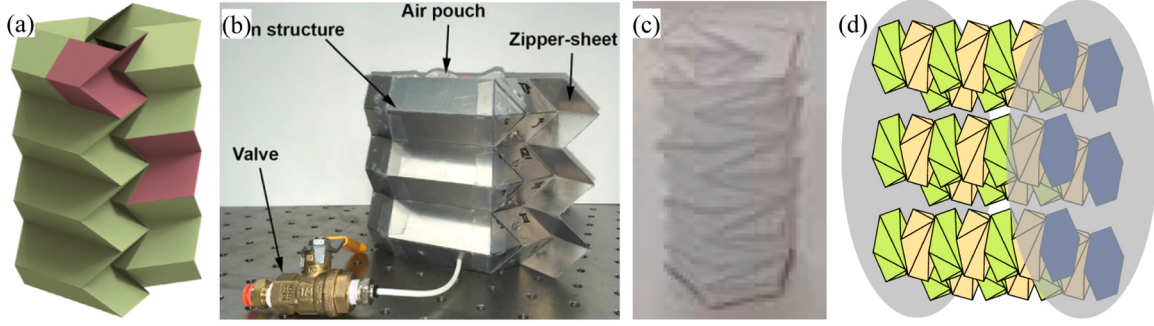


Fig. 7. QZS isolators based on origami structures; (a) Tachi-Miura origami; (b) Miura origami with fluid inside; (c) Kresling origami; (d) parallel connection of Kresling origamis.

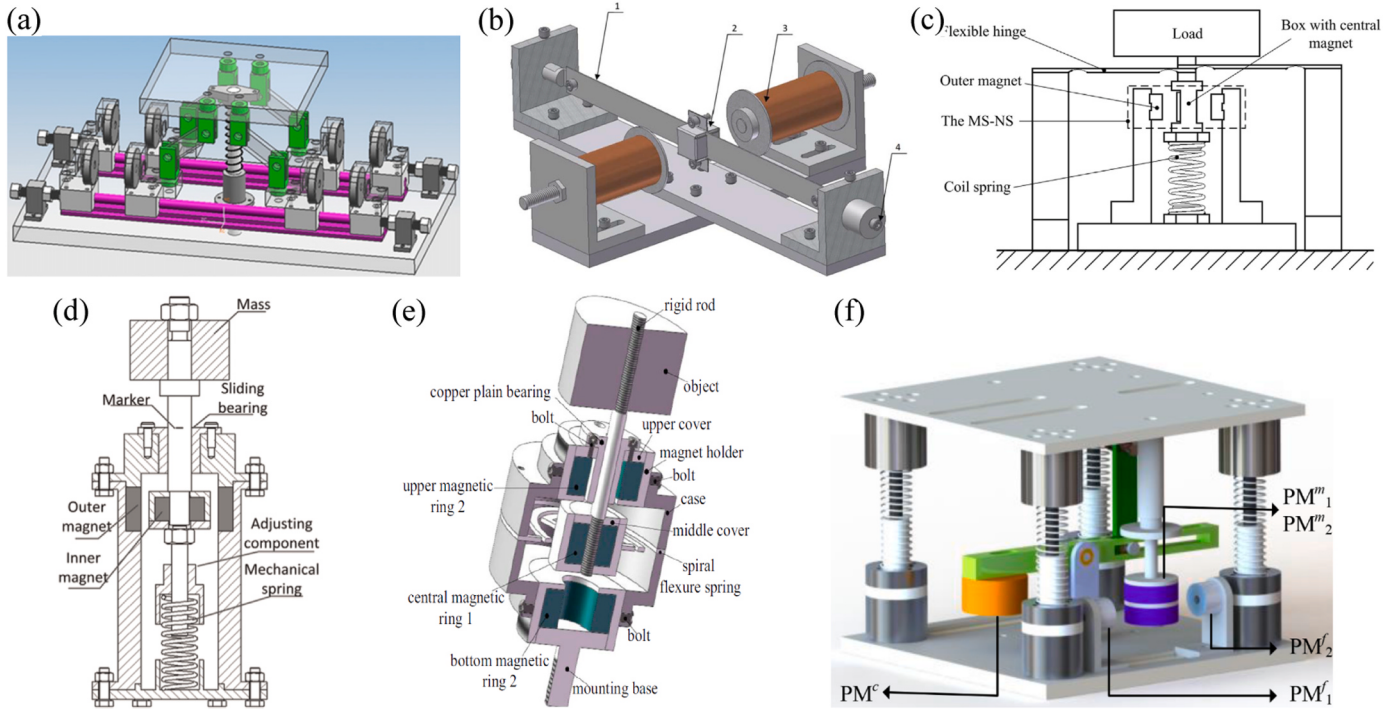


Fig. 8. Magnetic QZS isolators: (a) using permanent magnets and linkages; (b) using electromagnets and beam; (c) using cuboid-shaped magnets; (d) using radially magnetized ring-shaped magnets; (e) using axially magnetized ring-shaped magnets; (f) using axially magnetized ring-shaped magnets with non-coaxial arrangement.

magnetic force and displacement is proportional to the area of the end face perpendicular to the direction of magnetization. Wu et al. [73]

The generated magnetic restoring force for this arrangement calculated by the equivalent magnetic charge method is

$$F_{\text{magnet}} = \frac{JJ'}{2\pi\mu_0} \sum_{i=0}^1 \sum_{j=0}^1 \sum_{k=0}^1 \sum_{l=0}^1 \sum_{p=0}^1 \sum_{q=0}^1 (-1)^{i+j+k+l+p+q} \left[\frac{V_{kl}^2 - W_{pq}^2}{2} \ln \left(\sqrt{U_{ij}^2 + V_{kl}^2 + W_{pq}^2} - U_{ij} \right) \right. \\ \left. + U_{ij} V_{kl} \ln \left(\sqrt{U_{ij}^2 + V_{kl}^2 + W_{pq}^2} - V_{kl} \right) + V_{kl} W_{pq} \arctan \frac{U_{ij} V_{kl}}{r W_{pq}} + \frac{\sqrt{U_{ij}^2 + V_{kl}^2 + W_{pq}^2}}{2} U_{ij} \right] \quad (9)$$

utilized a floating cuboid-shaped magnet to interact with two fixed cuboid-shaped magnets to produce negative stiffness, and then connected it in parallel with a spring to build a QZS isolator as shown in Fig. 8(c). In this isolator, the three magnets had the same magnetization direction perpendicular to the vibration direction, and the two fixed magnets had the same polarity opposite to that of the floating magnet.

where $U_{ij} = x + (-1)^j a' - (-1)^i a$, $V_{kl} = (-1)^l b' - (-1)^k b$, $W_{pq} = h + (-1)^q c' - (-1)^p c$. Sun et al. [74] employed two pairs of plate magnets (i.e. the cuboid-shaped magnet with a small size in a certain direction) magnetized in the thickness direction to construct a local QZS isolator, which is essentially arranged in the same way as that in Ref. [73], but its

positive stiffness element is a cantilever beam instead of a coil spring. Wu et al. [75] used an array of cuboid-shaped magnets to design a magnetic QZS isolator, in which the magnetization direction of all magnets is perpendicular to the vibration direction and the polarities of adjacent magnets (whether horizontally adjacent or vertically adjacent) are opposite.

2.3.3. Using ring-shaped magnets

The ring-shaped magnets utilized for constructing the QZS isolator are generally arranged in a coaxial configuration, and the magnetization direction mainly includes radial magnetization and axial magnetization.

Since it is difficult to conduct radial magnetization for a ring-shaped magnet, we can employ multiple radially magnetized tiles to equivalently form a radially magnetized ring. Zheng et al. [76] arranged two radially magnetized ring-shaped magnets with opposite polarities coaxially and formulated the expression for the magnetic restoring force by using the Ampere molecular current model as

$$F_{\text{magnet}} = - \sum_{i=1}^2 \sum_{j=3}^4 \left[\frac{\mu_0 k_s^2 h_{ij}}{4\pi} \int_{R_1}^{R_1+T_1} \int_{R_2}^{R_2+T_2} \int_0^{2\pi} \right. \\ \times \left. \int_0^{2\pi} \frac{r_1 r_2 \cos(\theta_2 - \theta_1)}{\left(r_2^2 + r_1^2 + h_{ij}^2 - 2r_1 r_2 \cos(\theta_2 - \theta_1) \right)^{3/2}} dr_1 dr_2 d\theta_1 d\theta_2 \right] \quad (10)$$

where $h_{ij}(H) = (-1)^{i+j} H - (-1)^j L_1 + (-1)^i L_2$. This arrangement can produce magnetic negative stiffness in the axial direction and thus is connected with a spring in parallel to build a QZS isolator, as shown in Fig. 8(d). They also designed a torsional QZS isolator using ring-shaped magnets composed of multiple radially magnetized tiles with interlaced magnetization directions for negative stiffness and a rubber spring for positive stiffness [77]. Xu et al. [78] exploited this magnetic torsional QZS isolator for the torsional vibration isolation of a joint actuator.

Dong et al. [79] designed a magnetic QZS isolator by using three axially magnetized ring-shaped magnets and a spiral flexure spring, in which two fixed magnets and one floating magnet are arranged coaxially with the same polarity, as shown in Fig. 8(e). The expression for the axial magnetic restoring force of this isolator is

$$F_{\text{magnet}}(z) = \frac{\mu_0 M_1 M_2 z}{4\pi} \sum_{i=1}^2 \sum_{k=1}^2 (-1)^{i+k} \int_0^{2\pi} \\ \times \int_0^{2\pi} \left[\int_{l+\frac{h_1}{2}}^{l+\frac{h_1}{2}+h_2} (\Phi_2 - \Phi_1) dz_2 + \int_{-\frac{h_1}{2}-l-h_2}^{-\frac{h_1}{2}-l} (\Phi_2 - \Phi_1) dz_2 \right] d\varphi_2 d\varphi_1 \quad (11)$$

where

$$\Phi_1 = \frac{\cos(\varphi_2 - \varphi_1) r(i) r_{in2}}{\sqrt{r_{in2}^2 + r^2(i) - 2r_{in2}r(i)\cos(\varphi_2 - \varphi_1) + (z_2 - z(k))^2}} \quad (12)$$

$$\Phi_2 = \frac{\cos(\varphi_2 - \varphi_1) r(i) r_{out2}}{\sqrt{r_{out2}^2 + r^2(i) - 2r_{out2}r(i)\cos(\varphi_2 - \varphi_1) + (z_2 - z(k))^2}} \quad (13)$$

The magnetic stiffness is negative in a certain displacement range, while the stiffness of the spiral flexure spring is positive, so the QZS property can be obtained by their parallel combination. Wang et al. [80] designed a compact QZS isolator using two axially magnetized ring-shaped magnets with a coaxial arrangement, which is similar to that in Ref. [79]; the difference is that only one fixed magnet is utilized and the positive stiffness element is a waveform spring. In addition to the coaxial arrangement, axially magnetized ring-shaped magnets can also be configured in a non-coaxial manner to generate magnetic negative stiffness. Yan et al. [81] designed a lever-type magnetic QZS

isolator as shown in Fig. 8(f) by utilizing several non-coaxially arranged ring-shaped magnets, where the role of the lever is to increase inertia and thus further reduce the resonant frequency. The negative stiffness is generated by four axially magnetized ring-shaped magnets, in which two fixed magnets are coaxial with their axis perpendicular to the vibration direction and two moving magnets are coaxial with their axis oriented in the vibration direction. An additional permanent magnet is also attached at the free end of the lever to produce eddy current damping to suppress the undesirable jump phenomenon.

2.4. Other construction approaches

Geometric nonlinearity, magnetic nonlinearity, and nonlinearity in deformable components are three categories of the most commonly used approaches for constructing QZS isolators, while there are also some infrequent approaches employed by researchers.

Palomares et al. [82] employed three pneumatic springs to construct a QZS isolator as shown in Fig. 9(a). In this isolator, the vertical pneumatic spring provides positive stiffness and bears the vibration isolation object, while the combination of lateral pneumatic springs provides negative stiffness in the vertical direction, which is essentially similar to the three-spring QZS isolator in Fig. 2(a), except that the pneumatic spring itself has nonlinear stiffness characteristics. In the theoretical modeling, the vertical pneumatic spring is simplified as a spring with stiffness k without consideration of its polytropic process, while the polytropic process of the lateral pneumatic spring is considered ($PV^n = \text{const}$ with n the polytropic index), which leads to the following expression that describes the restoring force of the whole isolator:

$$f_{\text{res}}(z) = kz - 2A_e \left[P_0 \left(\frac{d_0}{d_0 + \sqrt{L_0^2 + z^2} - L_0} \right)^n - P_a \right] \frac{z}{\sqrt{L_0^2 + z^2}} \quad (14)$$

where A_e is the effective area of the lateral pneumatic spring, P_0 is the initial pressure, P_a is the ambient pressure, L_0 is the horizontal displacement between the actuator joints, and d_0 is the initial compression of the lateral pneumatic spring. Similarly, An et al. [83] changed the linear springs in the spring-linkage type QZS isolator to the pneumatic springs and studied the pneumatic QZS isolator with mistuned mass, revealing that a larger excitation force will lead to richer nonlinear dynamic behaviors and that increasing damping can inhibit the formation of chaotic motion. Vo et al. [84] designed a QZS isolator as shown in Fig. 9(b) by using four pneumatic springs, in which the negative stiffness is produced by the lower pneumatic springs and the cam-roller mechanism and the positive stiffness is produced by the upper pneumatic springs and the bevel-roller mechanism. Moreover, the static equilibrium position of this QZS isolator for different loads can be set in a predetermined position by adjusting the initial internal pressure of the upper pneumatic springs.

Meng et al. [85] designed the structural parameters of a disk spring to obtain the QZS characteristic, and Chen et al. [86] utilized the disk-spring-based QZS element as a nonlinear energy sink (NES) for vertical vibration control. Gao et al. [87] employed a bellows container with solid-liquid mixture inside to design an HSLDS isolator, as shown in Fig. 9(c), in which the elastic solid granules are hollow with the initial internal pressure equal to the atmospheric pressure. Within a certain displacement range, the elastic solid granules expand or contract with the deformation of the bellows container, and the restoring force of the isolator is produced by both the bellows container and the elastic solid granules. When the displacement is larger than a critical value, the elastic solid granules always remain in the equilibrium state, and therefore only the bellows container is responsible for the restoring force of the isolator, resulting in relatively small stiffness. Consequently, the stiffness of the solid-liquid mixture type HSLDS isolator is a piecewise function:

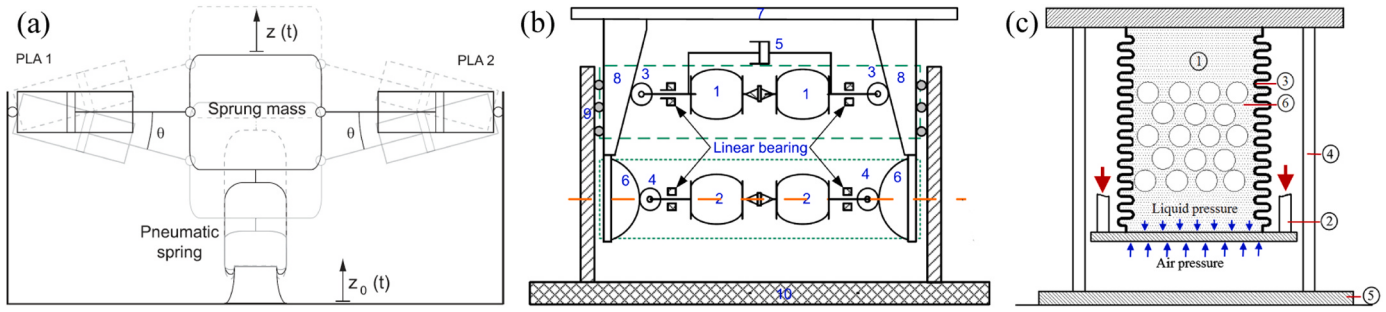


Fig. 9. (a) QZS isolator using pneumatic springs and linkages; (b) QZS isolator using pneumatic springs and rollers; (c) HSLDS isolator using solid-liquid mixture.

$$K(x) = \begin{cases} K_2 + \frac{S_e^2}{NA_e} \left[K_{ep} + \frac{P_a L (NA_e)^2}{(LNA_e + S_e x)^2} \right] x < x_c \\ K_2 x > x_c \end{cases} \quad (15)$$

where the expression for the critical displacement is \$x_c = NA_e y_c / S_e\$. The static equilibrium point when loaded is designed in the range of \$x > x_c\$, and thus a small stiffness can be obtained in the vicinity of the static equilibrium point.

3. MDOF QZS vibration isolation systems

3.1. One-piece type MDOF QZS isolators

The key to the design of a one-piece type MDOF QZS isolator is to construct a structure or mechanism that can achieve QZS characteristic in multiple DOFs or directions. In general, the restoring forces (restoring moments) in multiple DOFs are coupled to each other, and the stiffness of each DOF is defined as the first-order derivative of each restoring

force (restoring moment) with respect to the displacement (angular displacement) in the corresponding DOF. In recent years, a number of one-piece type MDOF QZS isolators have been proposed for different kinds of MDOF vibration excitations.

3.1.1. Two-directional translational one-piece type QZS isolators

Liu et al. [88] designed a magnetic in-plane QZS isolator by using two radially magnetized ring-shaped magnets (assembled by multiple magnetic tiles) and eight pre-tensioned cables, as shown in Fig. 10(a). The two ring-shaped magnets have the same magnetization direction, which can produce isotropic negative stiffness in any direction in the horizontal plane. The eight pre-tensioned cables can produce positive stiffness in any direction in the horizontal plane, and therefore the combination of the magnets and cables can produce quasi-zero stiffness in the horizontal orthogonal direction by proper parameter design, achieving low-frequency vibration isolation in two horizontal orthogonal directions, or in other words in any direction in the horizontal plane (note that the vibration in any direction in the horizontal plane can be

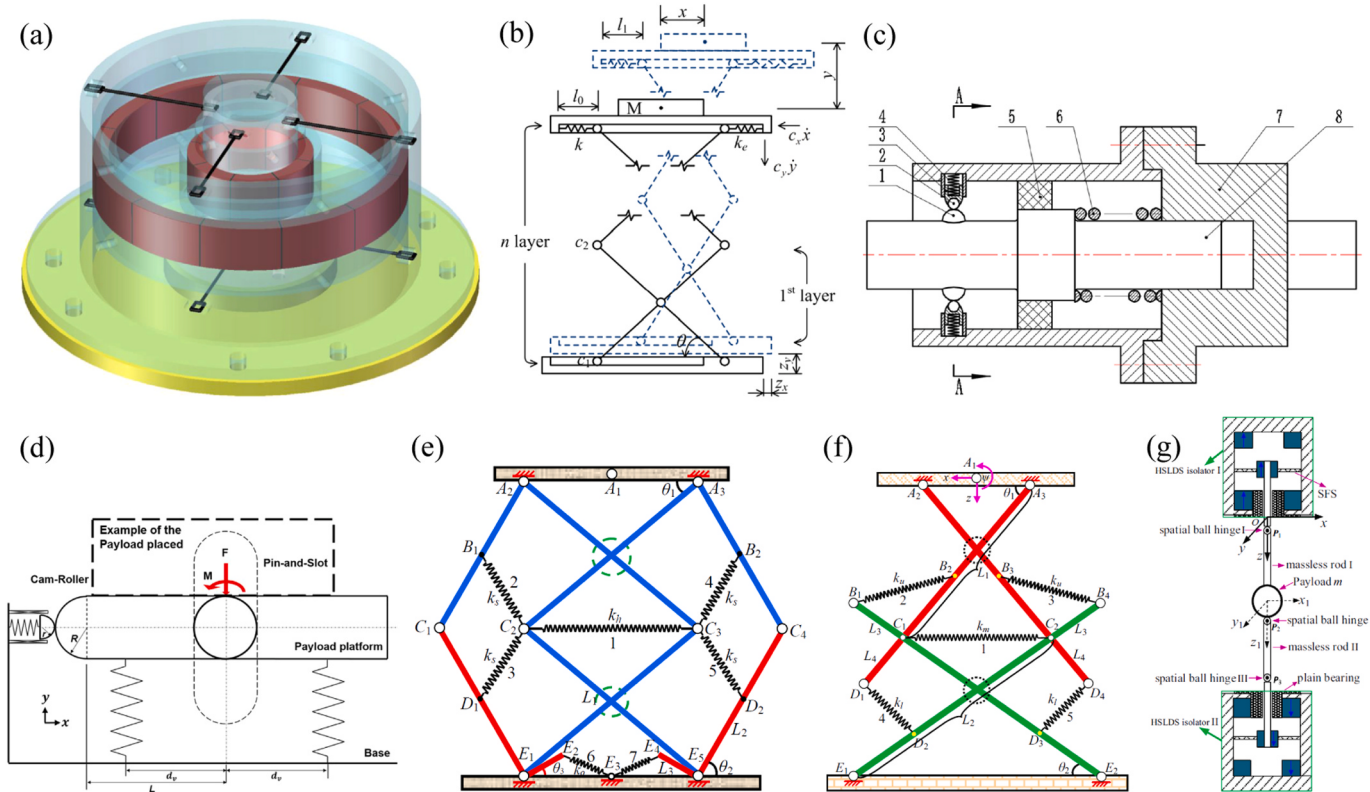


Fig. 10. One-piece type MDOF QZS isolators: (a) in-plane magnetic QZS isolator; (b) two-directional QZS isolator based on scissor-like stricture; (c) QZS isolator for torsional and axially translational coupled vibrations; (d) QZS isolator for translational and rotational coupled vibrations; (e) QZS isolator for coupled vibrations in two translational directions and a rotational direction; (f) three-directional QZS isolator based on spatial pendulum.

decomposed into two given orthogonal directions). Sun et al. [89] added a horizontal spring in the uppermost layer of the scissor-like structure to obtain a two-directional QZS isolator for isolating the vibrations in both vertical and horizontal directions, as shown in Fig. 10(b), which has high-static-low-dynamic stiffness in the vertical direction, resulting in a low first-order "natural frequency"; besides, an anti-resonance band can be obtained between the two "natural frequencies" via the design of structural parameters.

3.1.2. Translational-rotational coupled one-piece type QZS isolators

Zhang et al. [90] designed a torsional-translational QZS isolator for shaft by using spherical cams, spherical rollers and springs, as shown in Fig. 10(c). The interaction between the spherical cam and the spherical roller supported by the radial spring can produce not only torsional negative stiffness but also axial translational negative stiffness, which are then combined with the rubber spring with torsional positive stiffness and the axial spring with translational positive stiffness respectively, thus achieving quasi-zero stiffness in both the torsional DOF and axial translational DOF. Ye et al. [91] also designed a QZS isolator for coupled translational and rotational vibrations based on the cam-roller-spring mechanism, as shown in Fig. 10(d), differing from the design of Zhang et al. in that the direction of the rotation vector is perpendicular to the translational direction rather than coaxial.

3.1.3. Two-directional translational and rotational coupled one-piece type QZS isolators

Chai et al. designed two kinds of MDOF QZS isolators [92,93] for both two-directional translational vibration isolations and rotational vibration isolation. The former utilized ten linkages and seven springs, where two pairs of adjacent linkages (marked in red) are rigidly connected to each other, as shown in Fig. 10(e), and the latter utilized four linkages and five springs, as shown in Fig. 10(f). Due to the geometric nonlinearity, this QZS isolator can produce asymmetric quasi-zero stiffness in the vertical direction and symmetric lower stiffness in the horizontal and rotational directions, thus achieving low-frequency vibration isolation in two translational DOFs and a rotational DOF.

3.1.4. Three-directional translational one-piece type QZS isolators

Dong et al. [94] designed a three-directional translational QZS isolator as shown in Fig. 10(g) using the spatial double pendulum mechanism and two QZS supports. Each QZS support is composed of two fixed axially magnetized ring-shaped magnets, a movable axially

magnetized ring-shaped magnet, and a spiral flexure spring, which has the same principle as the QZS isolator shown in Fig. 8(e). The combination of the spatial double pendulum and the QZS supports can achieve quasi-zero stiffness in the two horizontal directions and the vertical direction, thus achieving low-frequency vibration isolation in the three orthogonal directions.

3.2. Platform type 6DOF QZS isolation systems

The QZS isolator can be converted into the QZS strut, and several QZS struts can be utilized as legs to build the QZS isolation platform for achieving 6DOF low-frequency vibration isolation. There are two key points in the design process of the QZS vibration isolation platform. The first point is the stiffness characteristics of the strut, and the second point is the layout of the legs. In general, if the strut acting as the leg possesses QZS characteristic, the vibration isolation platform possesses QZS characteristic in all six DOFs.

There are many ways to construct QZS struts, similar to the ways of constructing QZS isolators as mentioned in Section 2. Tuo et al. [95] utilized the three-spring mechanism to design a QZS strut; Yang et al. [96] and Liu et al. [97] utilized springs and linkages to design the QZS strut shown in Fig. 11(a) and the HSLDS strut shown in Fig. 11(b) respectively, in which the combination of horizontal spring(s) and linkages produces negative stiffness in the axial direction of the strut, while the vertical spring provides positive stiffness. Zhou et al. [98] designed a QZS strut as shown in Fig. 11(c) by replacing the horizontal springs in the cam-roller-spring mechanism with three clamped-clamped beams to reduce the overall size. The above-mentioned four kinds of QZS/HSLDS struts are all based on geometric nonlinearity. Liu et al. [99] designed a QZS strut as shown in Fig. 11(d) by using a disc spring with bi-stability (the disc spring is in the buckled state at the unstable equilibrium point) to provide negative stiffness and a coil spring to provide positive stiffness. Zhou et al. [100] and Zheng et al. [101] designed the magnetic QZS struts as shown in Fig. 11(e) and (f) respectively based on magnetic nonlinearity by using the ring-shaped magnets. The difference between both designs lies in the magnetization direction. The former is axially magnetized, while the latter is radially magnetized.

It is essential to design the layout of legs for the vibration isolation platform built from the QZS/HSLDS struts. The most classical layout is the Stewart configuration as shown in Fig. 12(a), which has been adopted in Refs.[95,101]. In addition to the Stewart configuration, Ref.

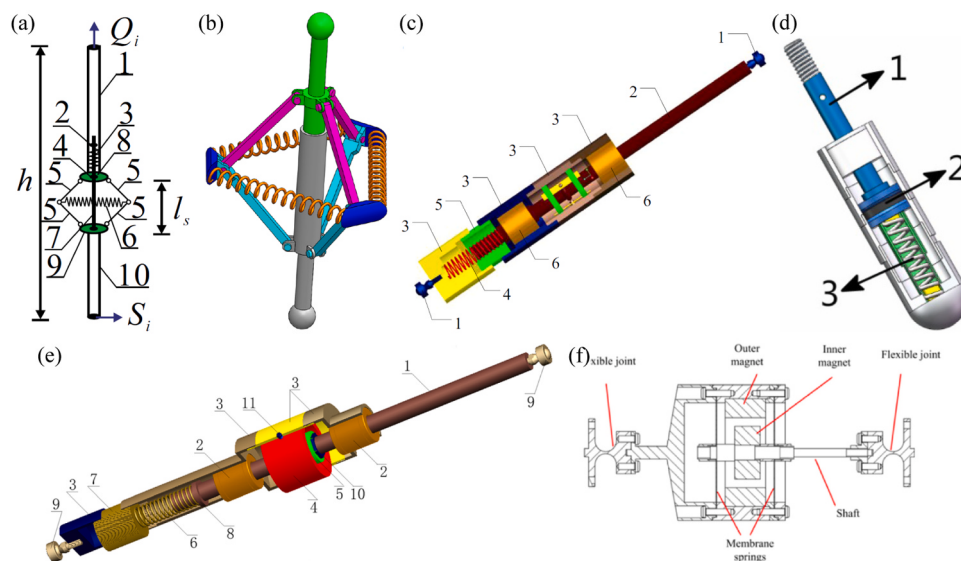


Fig. 11. QZS/HSLDS struts: (a) QZS strut using springs and linkages; (b) HSLDS strut using springs and linkages; (c) QZS strut using cams, rollers, spring and beams; (d) QZS strut using disc spring; (e) QZS strut using axially magnetized ring magnets; (f) QZS strut using radially magnetized ring magnets.

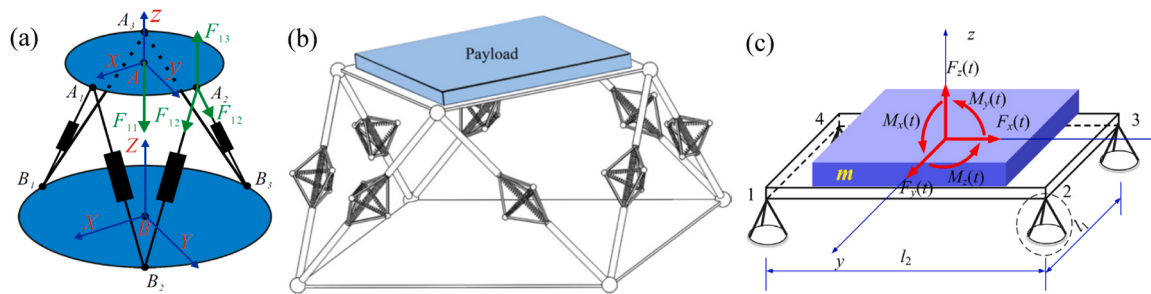


Fig. 12. Layouts of legs for 6DOF vibration isolation platform; (a) Stewart configuration; (b) eight-legged orthogonal configuration; (c) four-cornered pyramid configuration.

[97] used an eight-legged orthogonal configuration as shown in Fig. 12(b), which allows the linear part of the dynamic equations to be completely decoupled (but the nonlinear part is still unavoidably coupled), and Refs.[98,99] used a four-cornered pyramid configuration as shown in Fig. 12(c), which reduces the height of the platform and has high reliability due to many legs.

4. Improvement strategies for QZS isolators

4.1. Broadening the low-stiffness displacement range

In general, the dynamic stiffness (tangent slope) of the QZS isolator at the static equilibrium point is zero (or tends to zero). With the increase in the displacement from the static equilibrium point, the stiffness generally increases gradually. When the displacement increases to a certain extent, the system no longer has a small dynamic stiffness, and its stiffness may even be larger than that of the equivalent linear isolator. For a pre-given small stiffness value, there exists a displacement range corresponding to it, in which the dynamic stiffness is lower than the pre-given small stiffness value, and thus this displacement range can be called the low-stiffness displacement range. Obviously, to achieve the best vibration isolation performance, the width of the low-stiffness displacement range should be extended as far as possible. A number of researchers have put efforts into broadening the low-stiffness displacement range.

4.1.1. Increasing the number of design parameters

Zhao et al. modified the three-spring QZS isolator by increasing the number of pair(s) of oblique springs from one to two [102] and three [103] respectively, as shown in Fig. 13(a) and (b). The restoring force–displacement relationship of the three-spring QZS isolator has two dimensionless parameters (geometric ratio and stiffness ratio), only one of which is independent if the QZS condition is satisfied. The displacement range in which the dimensionless stiffness is lower than the pre-given stiffness value \hat{K}_0 is $|\hat{x} - \hat{x}_e| < \gamma\sqrt{[1 - \hat{K}_0(1 - \gamma)]^{-2/3} - 1}$ [14] where $\gamma = a/L_0$ and the stiffness ratio α is dependent on γ to satisfy the QZS condition ($\alpha_{QZS} = \gamma/[2(1 - \gamma)]$). By increasing the number of pair(s) of oblique springs, the number of dimensionless parameters is also increased accordingly, allowing parameter optimization to broaden the low-stiffness displacement range on the premise of satisfying the QZS condition [104], as shown in Fig. 13(c) and (d). Taking the QZS isolator with three pairs of oblique springs as an example, it has five dimensionless parameters (three geometric ratios and two stiffness ratios). On the premise of satisfying the QZS condition, it has four independent dimensionless parameters. Based on the principle of high-order quasi-zero stiffness [105], the low-stiffness displacement range can be further extended by letting the third-order derivative of the restoring force with respect to displacement be zero at the static equilibrium point [106]. Similarly, by changing the positive stiffness element from a single vertical spring to the combination of two oblique springs [107] or the

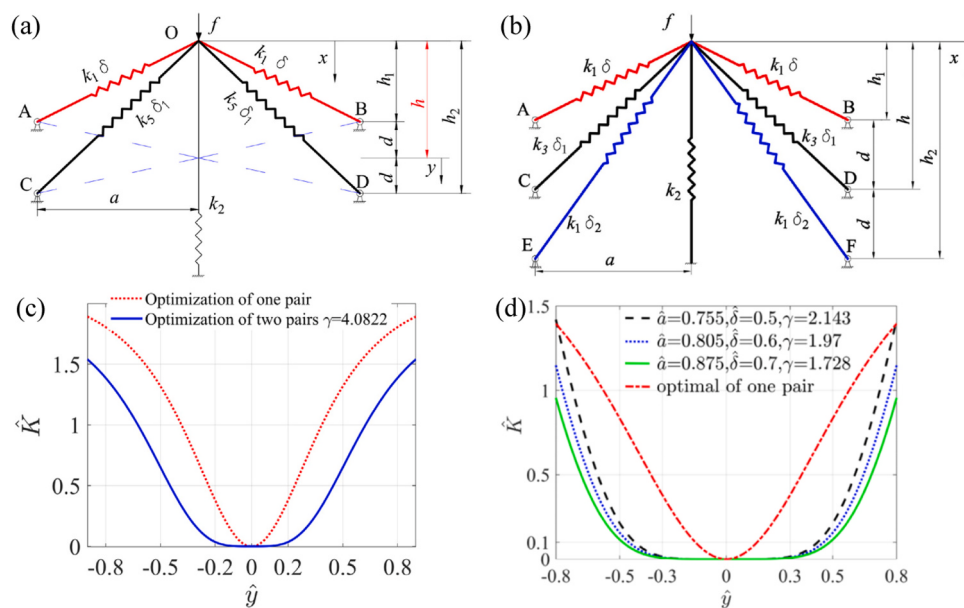


Fig. 13. Increasing the number of pairs of oblique springs to broaden the low-stiffness displacement range: (a) using two pairs of oblique springs; (b) using three pairs of oblique springs; (c) stiffness-displacement relationship using two pairs of oblique springs and its comparison with the case of one pair of oblique springs; (d) stiffness-displacement relationship using three pairs of oblique springs and its comparison with the case of one pair of oblique springs.

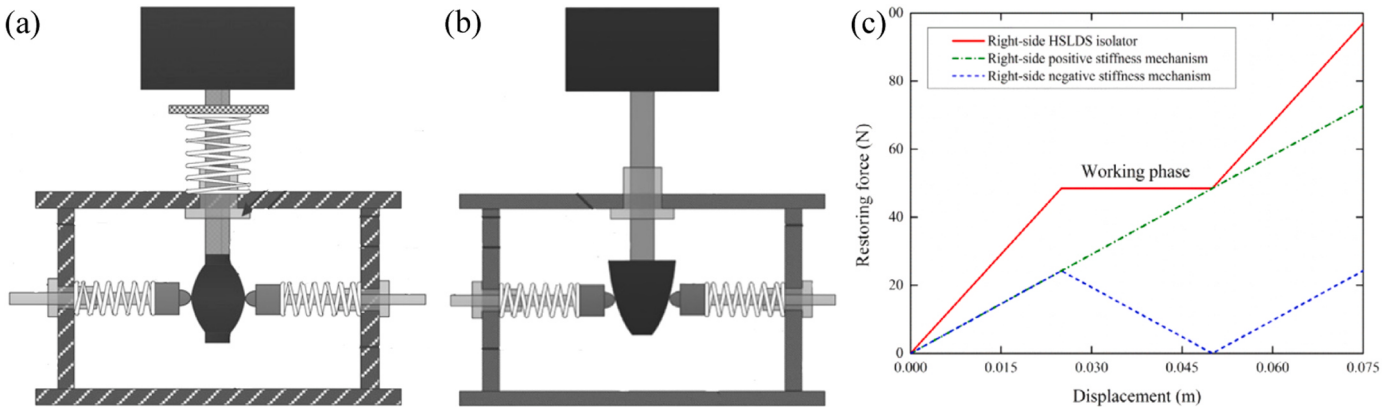


Fig. 14. Designing the cam profile to broaden the low-stiffness displacement range: (a) incorporating vertical spring; (b) removing vertical spring; (c) piecewise linear restoring force—displacement relationship obtained by the reverse design of the cam profile.

combination of torsional springs and oblique bars [108], the number of design parameters can also be increased to permit optimization for a broader low-stiffness displacement range.

4.1.2. Reverse designs

In the cam-roller-spring type QZS isolator, the circular cam is usually employed, while the non-circular cam (for example, the parabolic cam [109]) can actually give rise to more beneficial stiffness characteristics due to its designability. To broaden the low-stiffness displacement range for this kind of QZS isolator, Li et al. utilized non-circular cam to obtain the desired restoring force—displacement relationship by reversely designing the profile of the cam [110], as shown in Fig. 14(a). He also removed the vertical spring and obtained the desired restoring force—displacement relationship with broad low-stiffness displacement range by using the cam with user-defined profile [111], as shown in Fig. 14(b). Zou et al. [112] formulated a general mathematical expression for the reverse design of the cam profile to obtain any pre-given restoring force—displacement relationship:

$$S(x) = \sqrt{2 \int_0^x \frac{F(x) - Kx}{K_h} dx + x_0^2 - x_0} \quad (16)$$

where $F(x)$ is the pre-given restoring force—displacement relationship, K is the stiffness of the vertical spring (if there is no vertical spring, K is set to zero), K_h is the stiffness of the horizontal spring, and x_0 is the initial pre-compression of the horizontal spring. Yao et al. [113] designed the cam profile for producing a smooth and discontinuous piecewise linear restoring force—displacement relationship given in Fig. 14(c) based on Eq.(16); the stiffness is almost zero in a large displacement range around the static equilibrium point. Similar to the reverse design of the profile of the cam, Zhu et al. [114] designed a higher-order QZS isolator by using a reverse curve construction method, which can even achieve exact zero stiffness in a broad displacement range.

4.1.3. Other methods

Other kinds of QZS isolators can also be modified to broaden the low-stiffness displacement range. For example, Wang et al. [115] used the three-spring mechanism to replace the horizontal spring in the spring-linkage type QZS isolator to form a dual QZS vibration isolator, which has ultra-low stiffness in a wide displacement range around the static equilibrium point. Yan et al. [116] proposed a three-linkage mechanism with nearly linear negative stiffness in a large displacement range and then connected it in parallel with a vertical spring to obtain a large stroke QZS isolator with asymmetric stiffness characteristics. However, since the stiffness is decreasing over the working range, the stiffness at the static equilibrium point cannot be designed to zero

and must have a small positive value. Yuan et al. [117] changed the axially magnetized fixed ring-shaped magnet in Fig. 8(e) into the electromagnetic coil and added an extra electromagnetic coil at the same height of the floating magnet. The combined magnetic interactions between the three electromagnetic coils and the central floating magnet produce an approximately linear magnetic negative stiffness, making the whole isolator possess a very broad low-stiffness displacement range.

4.2. Nonlinear compensation method

The vast majority of QZS isolators employ the negative stiffness mechanisms with symmetric stiffness characteristics, and within a certain displacement range around the static equilibrium point, the restoring force of these negative stiffness mechanisms satisfies the following relationship:

$$x \frac{d^2 f_{res}}{dx^2} > 0 (x \neq 0 \text{ and } |x| < x_e) \quad (17)$$

That is to say, within a certain displacement range, the stiffness is increased with the absolute value of displacement. By using such negative stiffness mechanisms in parallel with positive stiffness elements to form QZS isolators, even though the stiffness at the static equilibrium point is designed to be zero, there is no negative stiffness in its neighborhood and thus the static instability does not exist. However, there is a class of asymmetric negative stiffness mechanisms whose restoring force—displacement function always satisfies $d^2 f_{res}/dx^2 < 0$ (such as the three-linkage mechanism in Ref.[116]), i.e., the stiffness decreases with an increasing displacement. For this class of negative stiffness mechanisms, if a linear positive element is employed to be connected in parallel with it, although the whole isolator can achieve low stiffness, the stiffness at the static equilibrium point cannot be designed to be zero and must have a small positive value (as shown in Fig. 15(a)) to avoid the static instability caused by the negative stiffness in the positive neighborhood of the static equilibrium point.

To resolve the deficiency of this class of negative stiffness mechanisms caused by the monotonically decreasing stiffness, Yan et al. proposed a nonlinear compensation method [118], the fundamental principle of which is to use the positive stiffness element with hardening nonlinearity to be connected in parallel with this class of negative stiffness mechanisms for the design of QZS isolator, as shown in Fig. 15 (b). Since the adopted positive stiffness element possesses hardening stiffness, when it is connected in parallel with the negative stiffness mechanism with monotonically decreasing stiffness, the stiffness in the positive neighborhood of the static equilibrium point could still be increased monotonically without static instability even if the stiffness at the static equilibrium point is designed to be zero. Yan et al. and Zhao

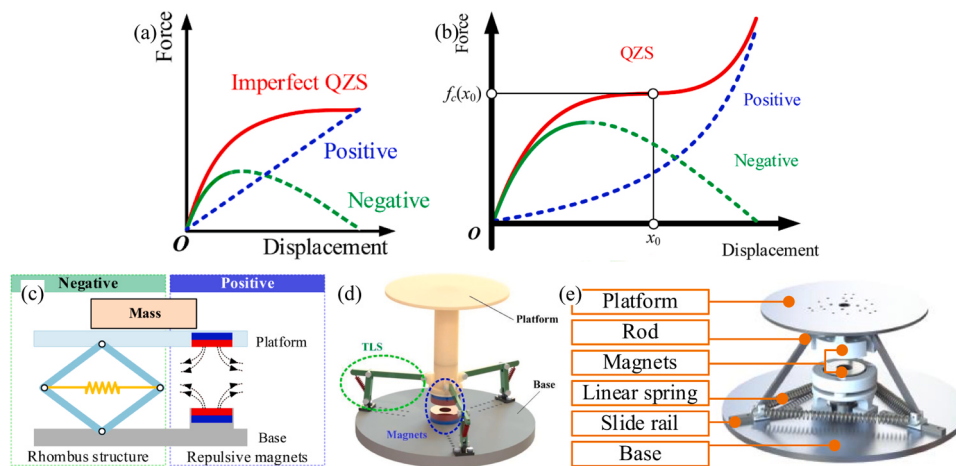


Fig. 15. Nonlinear compensation method and its implementation instances: (a) schematic diagram of the linear compensation method; (b) schematic diagram of the nonlinear compensation method; (c) first implementation instance; (d) second implementation instance; (e) third implementation instance.

et al. have also given three implementation instances of the nonlinear compensation method. In the first instance [118], the negative stiffness mechanism is composed of four linkages and a spring that constitute the rhombus structure, as shown in Fig. 15(c). In the second instance [119], the negative stiffness mechanism is a bionic structure inspired by the paw, as shown in Fig. 15(d). In the third instance [120], the negative stiffness mechanism is a tetrahedral structure composed of three linkages, three sliders and three springs as shown in Fig. 15(e). In all the three instances, the negative stiffness mechanism is based on geometric nonlinearity and has asymmetric characteristics with monotonically decreasing stiffness across the whole working range, and the positive stiffness mechanism is composed of two repulsive magnets to produce nonlinear hardening positive stiffness based on the inverse square law. The results validated that the utilization of the positive stiffness elements with nonlinear hardening characteristics can overcome the deficiency of the negative stiffness mechanism with monotonically decreasing stiffness.

4.3. Designs for supporting different loads

For QZS isolators, the static equilibrium position is determined by not only the structural design parameters but also the weight of the supported isolation object. It is best to make the static equilibrium point located at the pre-set position, since a deviation of the static equilibrium point would change the dynamic characteristics (for example, the appearance of an offset term in the response [121]) and thus influence the isolation performance. Some QZS isolators contain a specially designed adjustment mechanism [122] that corrects the static equilibrium position to handle the possible issue of system imperfection. The adjustment mechanism is useful for cases where the difference between the actual and presupposed weights is relatively small but not suitable

for an isolation object with a totally different weight. In other words, a QZS isolator designed for a certain load cannot provide effective vibration isolation for another load, since the new working range does not coincide with the designed QZS region and thus it no longer achieves the anticipated isolation performance. A fundamental way to support different loads is to design the QZS isolator with multiple allowable static equilibrium points, corresponding to different weights of the supported load.

Ye et al. [123] modified the cam-roller-springer type QZS isolator by employing multiple cams placed in the axial direction of the vertical rod, as shown in Fig. 16(a). Each cam corresponds to a specific static deflection of the vertical spring, rendering the system able to support multi-weight levels in their own QZS zones. The frictional force occurring on the cam-roller contact is considered in the modelling process to represent practical application situations. A stiffness “jump” was noticed at the ends of the effective zone, which may cause a high vibration level. To avoid the stiffness “jump”, the ineffective zones of each cam were removed, and the effective zones of different cams were joined together without any gap. Theoretical and experimental results showed that the designed QZS isolator with multiple cams can achieve good low-frequency isolation performance for several different weights of the isolation object. Zheng et al. [124] designed a QZS isolator composed of multiple series-arranged unit cells to acquire multiple QZS characteristics, as shown in Fig. 16(b). The unit cell is composed of a pair of semicircular arches and a pair of oblique beams; the former exhibits approximately linear positive stiffness under vertical force, and the latter is turned into buckled state when compressed vertically, thus generating negative stiffness. Each unit cell exhibits a single QZS characteristic, and therefore the restoring force—displacement relationship of the whole isolator designed by a series arrangement of them possesses multiple QZS zones, as shown in Fig. 16(c), which enables the existence

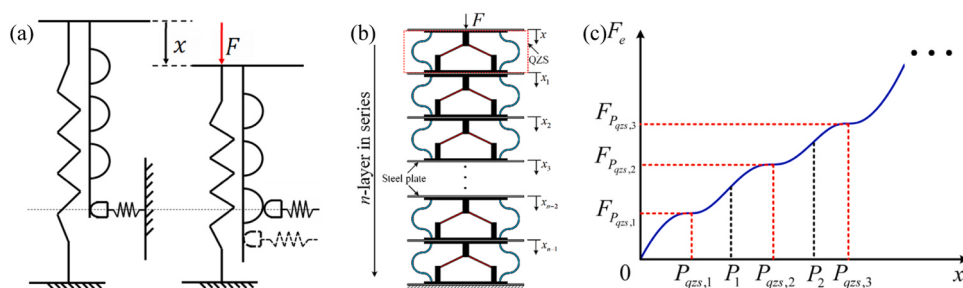


Fig. 16. Designs for supporting different loads: (a) cam-roller-springer type QZS isolator with multiple cams; (b) QZS isolator composed of multiple series-arranged QZS unit cells; (c) restoring force—displacement relationship.

of multiple static equilibrium points, corresponding to different weight levels of the isolation object. The results indicated that the dynamic behavior is related to not only structural parameters but also the preload and excitation amplitude and that increasing the number of layers is beneficial for the overall isolation performance.

4.4. Suppressing the rightward bending of resonance region

In general, QZS vibration isolators have hardening stiffness characteristics. For a hardening nonlinear system, the frequency response curve has a tendency to bend to the right, and this bending is especially severe under large excitation or small damping. When forward or backward frequency sweeping is conducted, the response amplitude and transmissibility will jump down or jump up at some critical frequencies [125], usually called the jump phenomenon [126]. In the frequency range between the jump-down frequency and the jump-up frequency, there exist three possible solution branches. The intermediate solution branch is unstable, and which of the upper or lower solution branch is taken depends on the initial conditions. If the excitation amplitude is small enough and the damping is large enough to ensure the nonoccurrence of the jump phenomenon, the vibration isolation frequency band starts from the “crossing frequency” (i.e. the frequency at which the transmissibility-frequency curve crosses the 0 dB line), resulting in a low isolation frequency and thus a good isolation performance. However, when the jump phenomenon exists, although the transmissibility of the lower solution branch is below the 0 dB line, the transmissibility of the upper solution branch is larger than 0 dB, which causes the vibration isolation effect to vanish at frequencies between the two jump frequencies, resulting in a reduced isolation frequency band. Although, theoretically, we can use the initial value control strategy [127] to make the initial conditions lie in the attraction basin for lower solution branch, the concrete implementation is difficult to achieve. In order to fundamentally resolve the deficiency of isolation region reduction caused by the jump phenomenon, it is necessary to suppress the rightward bending of the resonance region.

Liu et al. proposed introducing nonlinear auxiliary mass to the QZS isolator to suppress the rightward bending of the resonance region. The addition of nonlinear auxiliary mass does not mean adding a mass to the vibration isolation object but means attaching a mass (usually small mass compared to the isolation object) at a proper location in the vibration isolation structure to make the system have nonlinear inertia [128], which can therefore produce a significant influence on the dynamic response characteristics of the isolator. For the spring-linkage type QZS isolator, the nonlinear auxiliary mass can be attached on the linkages, as shown in Fig. 17(a), whose equation of motion is

$$\begin{aligned} & \left\{ m + 2m_a \left[\alpha^2 + \frac{(1-\alpha)^2 X^2}{L^2 - X^2} \right] \right\} \ddot{X} + 2m_a \frac{(1-\alpha)^2 L^2 X \dot{X}^2}{(L^2 - X^2)^2} + C \dot{X} \\ & + \left[K_v - 2K_h \left(1 - \frac{L - \delta_{h0}}{\sqrt{L^2 - X^2}} \right) \right] X = F_0 \cos(\Omega t) \end{aligned} \quad (18)$$

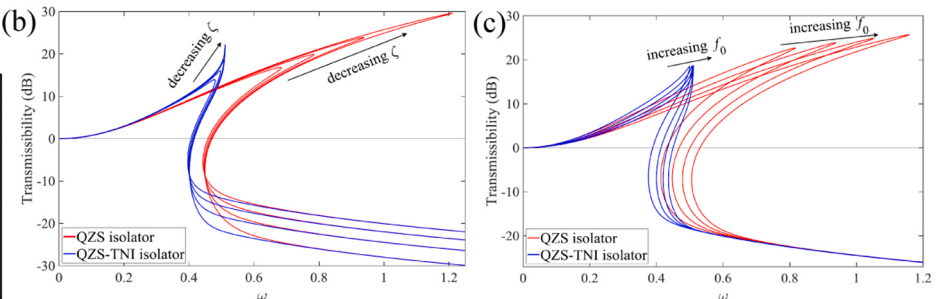
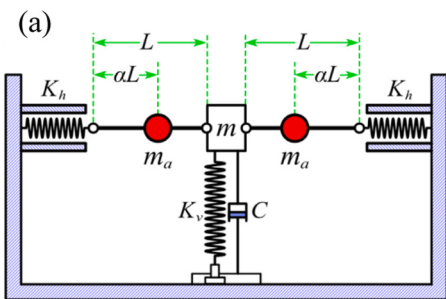


Fig. 17. Introducing nonlinear inerter to suppress the rightward bending of resonance region: (a) schematic diagram; (b) comparison with conventional QZS isolator in terms of the sensitivity to damping; (c) comparison with conventional QZS isolator in terms of the sensitivity to excitation amplitude.

It can be seen from Eq.(18) that the difference from the conventional QZS isolator lies in the nonlinear inertial term and an extra term as a nonlinear function of the displacement multiplied by the square of the velocity. The resonance region of the amplitude-frequency response curve of the QZS isolator with nonlinear auxiliary mass does not extend significantly to the right as the conventional QZS isolator does, so the rightward bending trend of the transmissibility curve is greatly suppressed, resulting in a much lower beginning frequency of vibration isolation than that of the conventional QZS isolator. The degree of sensitivity to the increase in the excitation amplitude or the decrease in the damping is much smaller than that of the conventional QZS isolator (as shown in Fig. 17(b)(c)), which ensures the capability to maintain a small beginning frequency of isolation even under a large excitation amplitude or small damping.

Liu et al. [129] also introduced an innerly suspended mass into the spring-linkage type QZS isolator, as shown in Fig. 18(a), to form a 2DOF linear-nonlinear isolator for eliminating the rightward bending of the resonance region. The essential difference from the dual-stage isolators to be discussed in the next subsection is that there is an additional elastic connection between the innerly suspended mass and the base frame. The core principle of this arrangement is to exploit linearity to suppress the side effect of nonlinearity, thereby effectively eliminating the rightward bending of the resonance region, as shown in Fig. 18(b)(c). The complete elimination of rightward bending has an extra benefit of producing a much lower peak transmissibility than the conventional QZS isolator.

4.5. Increasing the roll-off rate in high frequency region

The essential principle of the QZS isolator is to reduce the resonant frequency and thus reduce the beginning frequency of isolation, resulting in a broader vibration isolation frequency band; however, it has little effect on the high frequency transmissibility. In fact, for a SDOF vibration isolator with viscous damping, whether linear and nonlinear, the high frequency transmissibility approximately satisfies $T = 2\zeta/\omega$ [130] (ζ and ω represent the damping ratio and frequency respectively), which can also be written as $T(\text{dB}) = 20 \lg(2\zeta) - 20 \lg \omega$ in decibel form, indicating that the roll-off rate of high frequency transmissibility is 20 dB/dec. Obviously, a larger roll-off rate of high frequency transmissibility manifests better vibration isolation performance, which prompts researchers in this field to seek approaches for increasing the roll-off rate in high frequency region.

4.5.1. Dual-stage QZS isolation systems

The most intuitive way to increase the roll-off rate of high frequency transmissibility is based on the principle of dual-stage vibration isolation. The roll-off of each stage is 20 dB/dec, and therefore, after two stages of vibration isolation, the roll-off reaches 40 dB/dec. Lu et al. [131] studied a dual-stage QZS isolation system composed of two three-spring mechanisms and found that the nonlinearity in the upper stage has little effect on the transmissibility characteristics, while the nonlinearity in the lower stage has a significant effect. Wang et al. [132]

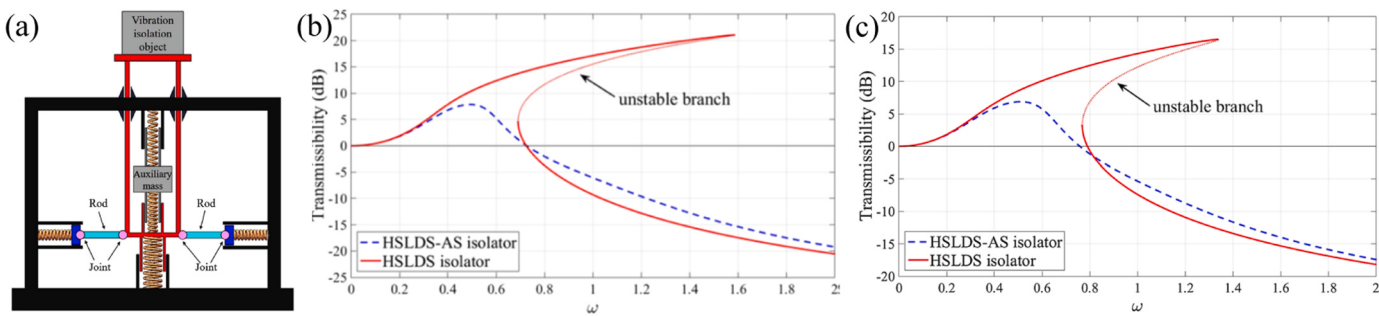


Fig. 18. Introducing internally suspended mass to suppress the rightward bending resonance region: (a) schematic diagram; (b) comparison with the conventional QZS isolator under a very small damping; (c) comparison with the conventional QZS isolator under a very large excitation amplitude.

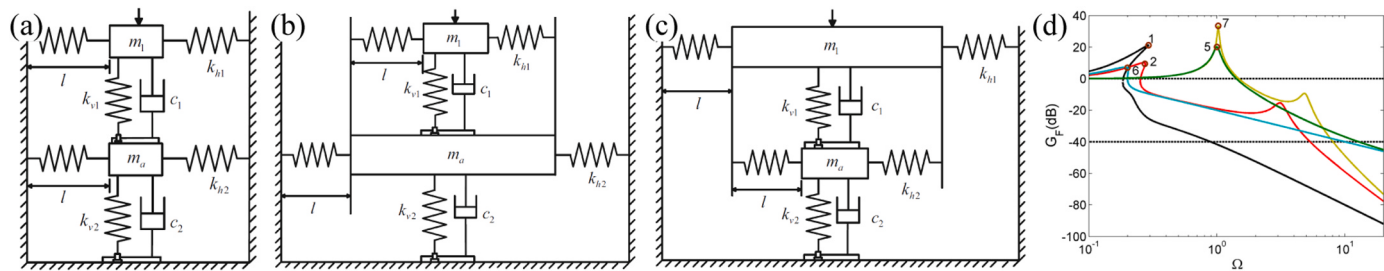


Fig. 19. Dual-stage QZS isolation system constituted by the three-spring mechanisms: (a) GG model; (b) BG model; (c) TG model; (d) transmissibility curve of the BG model and the comparison with the single-stage QZS isolator and the linear single-stage and dual-stage isolators.

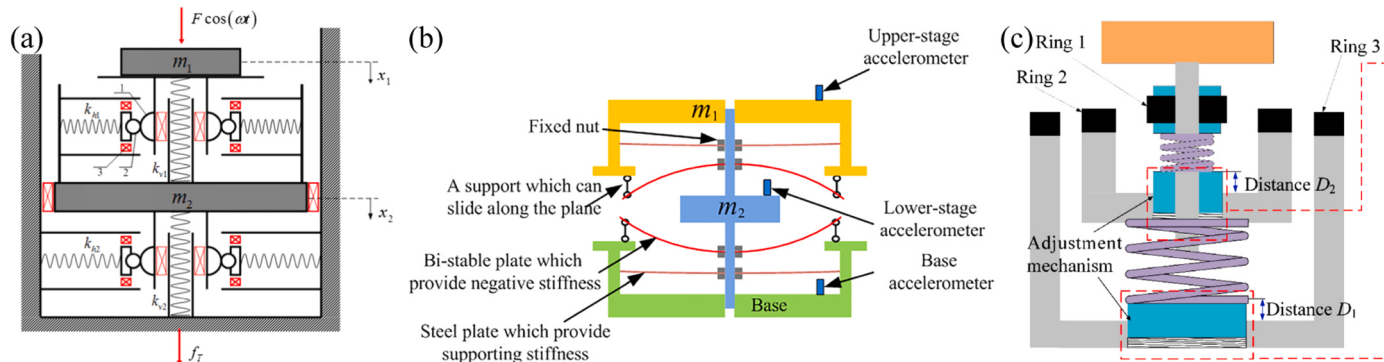


Fig. 20. Dual-stage QZS isolation systems constituted by other mechanisms: (a) using cam-roller-spring mechanisms; (b) using bi-stable carbon fiber reinforced laminates; (c) using axially magnetized ring-shaped magnets.

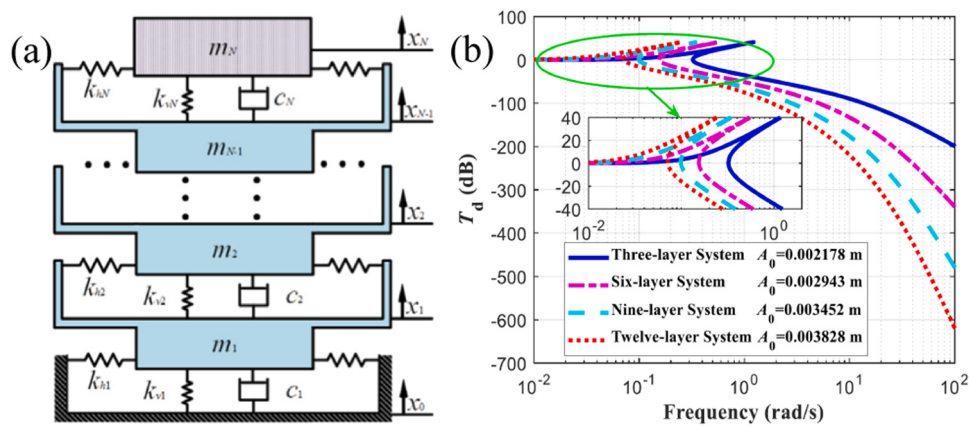


Fig. 21. Multi-stage QZS isolation system: (a) schematic diagram; (b) transmissibility curves of three-stage, six-stage, nine-stage and twelve-stage systems.

studied three kinds of configurations for the dual-stage QZS isolation system composed of three-spring mechanisms specifically, including the GG model, BG model and TG model, as shown in Fig. 19(a)(b)(c); they found that the BG model has better overall isolation performance than the GG and TG models, although the three models have the same roll-off rate for high frequency transmissibility. Fig. 19(d) presents the transmissibility curve of the BG model and the comparison with the single-stage QZS isolator and the linear single-stage and dual-stage isolators, which does indicate that the dual-stage isolation system has a larger roll-off rate than the single-stage isolator. In addition to the dual-stage QZS isolation system composed of three-spring mechanisms, Wang et al. [133], Lu et al. [134], and Wang et al. [135] constructed dual-stage QZS isolation systems by utilizing cam-roller-spring mechanisms, bi-stable carbon fiber reinforced laminates, and axially magnetized ring-shaped magnets, respectively, as shown in Fig. 20, all of which achieved a roll-off rate of 40 dB/dec for high frequency transmissibility.

4.5.2. Multi-stage QZS isolation systems

Obviously, if the number of stages of the vibration isolation system is further increased, the roll-off rate of high frequency transmissibility can be further increased accordingly. Deng et al. [136] utilized many three-spring mechanisms in series to design a multi-stage QZS vibration isolation system inspired by the multi-stage neck of birds, as shown in Fig. 21(a). The transmissibility curves in Fig. 21(b) indicate that the roll-off rate of high frequency transmissibility increases with the increase in the number of stages. It should be noted that the essential difference between the QZS isolator composed of multiple series-arranged QZS unit cells in Ref.[124] and the multi-stage QZS isolation system here lies in the degree of freedom: The former is modelled as a SDOF system since each cell unit is seen as a pure stiffness unit without consideration of the inertia of each unit, whereas the latter is a MDOF system that contains a lumped mass in each stage.

4.5.3. Viscoelastic QZS isolators

Instead of increasing the number of stages of the vibration isolation system, Liu et al. [137] took a totally different approach to increase the roll-off rate of high frequency transmissibility by introducing the Maxwell's viscoelastic damping into the single-stage QZS isolator, as shown in Fig. 22(a), the governing equation of motion of which is

$$\begin{aligned} \frac{mC}{NK_v}\ddot{X} + m\ddot{X} + \left[1 + \frac{1}{N} - \frac{2K_l}{NK_v} \left(\frac{L_0 L_h^2}{(L_h^2 + X^2)^{\frac{3}{2}}} - 1 \right) \right] C\dot{X} \\ + K_v X - 2K_l \left(\frac{L_0}{\sqrt{L_h^2 + X^2}} - 1 \right) X = F_0 \left[\cos(\Omega\tau) - \frac{\Omega C}{NK_v} \sin(\Omega\tau) \right] \end{aligned} \quad (19)$$

From the governing equation it can be seen that the introduction of Maxwell's viscoelastic damping makes the QZS isolator a third-order system. When the damping coefficient is not very large, the dynamic characteristics at low frequencies are similar to those of the conventional QZS isolator, but at high frequencies, the transmissibility rolls off

at twice the rate of the conventional QZS isolator, reaching 40 dB/dec, as shown in Fig. 22(b). Another feature of the viscoelastic QZS isolator is that the damping ratio has almost no effect on the high frequency transmissibility but has a significant effect at low frequencies. When increasing the damping ratio, the peak of the transmissibility curve is suppressed to the lower left; a further increase in the damping ratio can produce a new peak at a slightly higher frequency, as shown in Fig. 22(c). The optimum damping ratio occurs when the two peak values of transmissibility are equal, in which case the lowest peak transmissibility is obtained and the roll-off rate of high frequency transmissibility is maintained at 40 dB/dec, manifesting the benefits of introducing viscoelastic damping in both the high frequency region and resonance region.

4.6. Introducing nonlinear damping

Damping includes viscous damping, hysteresis damping, dry friction damping and other types. Liu et al. [138] pointed out that viscous damping can be divided into three categories: (1) linear viscous damping, whose damping force is a linear function of velocity, i.e. $F_c = cx$; (2) displacement-related nonlinear viscous damping, whose damping force can be written as the velocity multiplied by a nonlinear function of the displacement, i.e. $F_c = p(x)\dot{x}$; (3) displacement-unrelated nonlinear viscous damping, whose damping force is a nonlinear function of the velocity, i.e. $F_c = q(\dot{x})$. Most researchers have focused on the nonlinear stiffness characteristics in the design and theoretical modelling of QZS isolators, whereas the damping is usually designed as linear viscous damping. For the linear viscous damping, the variation of the damping coefficient causes the transmissibility in the resonance region and in the isolation region to vary inversely. Thus, it can never be achieved to optimize the vibration isolation performance in the whole frequency range by tuning the damping coefficient when employing linear viscous damping. To resolve the conflict between the transmissibility in the resonance region and that in the isolation region when designing damping, some researchers proposed introducing nonlinear damping characteristics into QZS isolators [139].

4.6.1. Hardening viscous damping

Qualitatively, the conflict between the isolation region and the resonance region when designing damping can be resolved if the introduced nonlinear damping characteristics can enable the coexistence of small damping in the isolation region and large damping in the resonance region. For displacement-related nonlinear viscous damping, this purpose can be achieved as long as $p(x)$ is designed as an increasing function of x , considering that the displacement in the resonance region is relatively large and the displacement in the isolation region is relatively small. Similar to the concept of hardening stiffness, the displacement-related nonlinear viscous damping in which $p(x)$ is an increasing function of x can be called "hardening viscous damping". The most commonly adopted principle for realizing hardening viscous damping is based on geometric nonlinearity, i.e. converting the linear

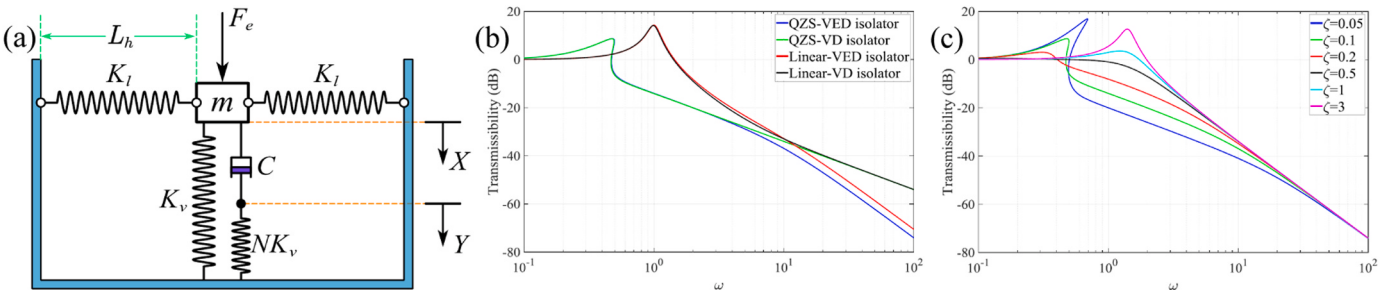


Fig. 22. Viscoelastic QZS isolator: (a) schematic diagram; (b) transmissibility curve and the comparison with the conventional QZS isolator, linear isolator and viscoelastic linear isolator; (c) variation of the transmissibility curve with the damping ratio.

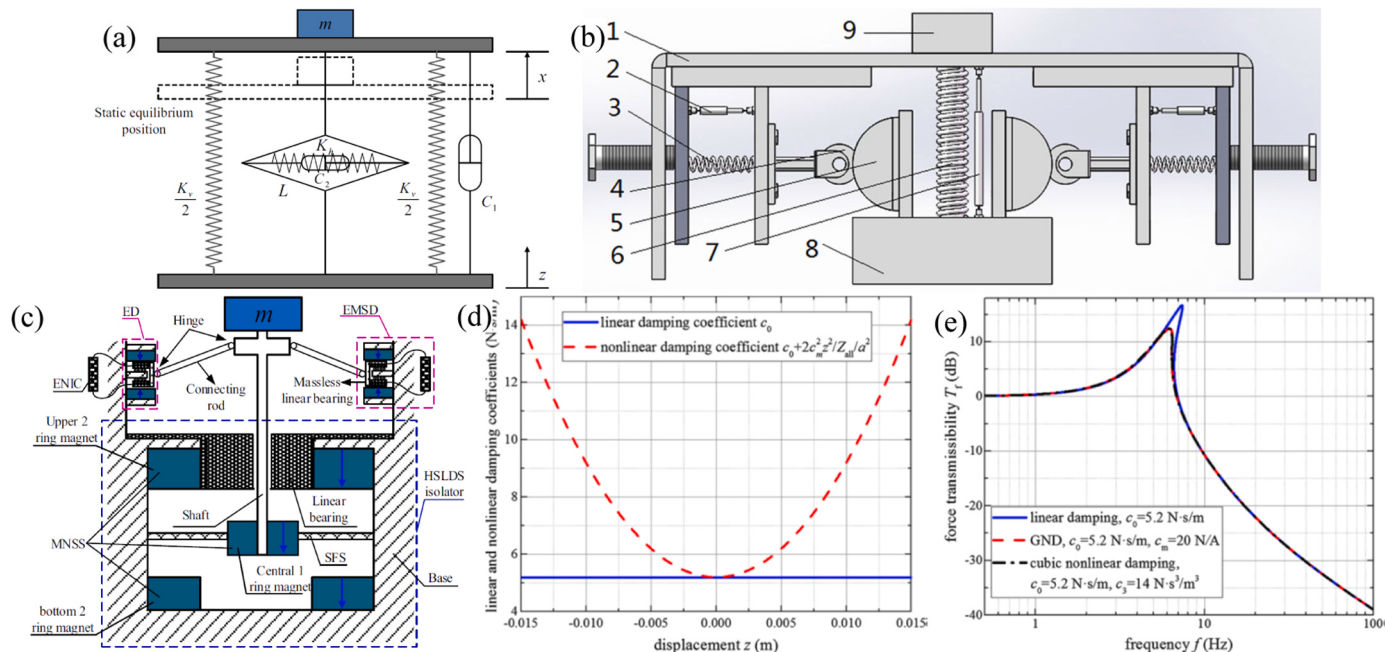


Fig. 23. QZS isolators with hardening viscous damping of the first kind based on geometric nonlinearity: (a) converted by linkages; (b) converted by cam-roll pairs; (c) electromagnetic hardening viscous damping converted by linkages (d) equivalent damping coefficient as a function of displacement; (e) transmissibility curve and comparison with the QZS isolator with linear viscous damping.

viscous damping in the non-vibration direction into the vibration direction through "rigid" components by means of reasonable mechanism designs. Cheng et al. [140] and Meng et al. [141] connected linear viscous damping in parallel with the horizontal spring of a spring-linkage type QZS isolator to convert the horizontal damping force into the vertical direction, as shown in Fig. 23(a). Liu et al. [142] connected linear viscous damping in parallel with the horizontal spring of the cam-roller-spring type QZS isolator, and the horizontal damping force was converted into the vertical direction through the cam-roll pairs, as shown in Fig. 23(b). Dong et al. [143] introduced horizontal electromagnetic damping into the magnet QZS isolator with axial magnetization, and the horizontal damping force was converted into the vertical direction through linkages, as shown in Fig. 23(c). The common feature of these implementations is that the conversion of horizontal linear viscous damping into the vertical direction through mechanical components produces hardening viscous damping. Taking the hardening viscous damping in Fig. 23(c) as an example, the expression for the damping coefficient is

$$c_{eq}(z) = c_0 + 2 \left(NR_p \int_0^{2\pi} B_{pr}(\varphi) d\varphi \right)^2 \frac{z^2}{Z_{all}a^2} \quad (20)$$

The damping coefficient is increased with the increase in the absolute value of displacement, as shown in Fig. 23(d), so as to reduce the peak transmissibility and suppress the resonant frequency without affecting the high frequency transmissibility, as shown in Fig. 23(e), thereby resolving the conflict between the resonance region and isolation region in the damping adjustment process to some extent.

Another way to realize hardening viscous damping is to construct proper piecewise damping. Hao et al. [144] placed a linear viscous damper at a certain distance above and below the static equilibrium position of the three-spring QZS isolator, as shown in Fig. 24(a), to produce piecewise linear viscous damping. Around the static equilibrium position ($-D_1 \leq x \leq D_2$), the damping coefficient is taken as a relatively small value C ; under large displacement ($x < -D_1$ or $x > D_2$), the damping coefficient is taken as a relatively large value $C + C_1$ or $C + C_2$. In a broad sense, this kind of piecewise damping belongs to the hardening viscous damping, and a strong degree of hardening can be achieved by choosing a small C and large C_1 and C_2 , thereby significantly suppressing the resonance peak and the rightward bending trend without affecting the high frequency transmissibility, as shown in Fig. 24(b).

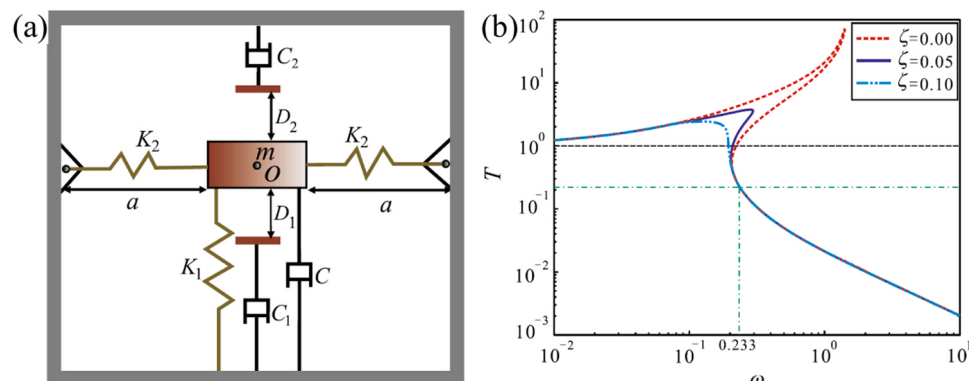


Fig. 24. QZS isolator with piecewise linear viscous damping: (a) schematic diagram; (b) variation of the transmissibility curve with the damping ratio.

4.6.2. Other kinds of nonlinear damping

The displacement-related hardening viscous damping is the most studied category of nonlinear damping for the performance enhancement of QZS isolators, while other types of nonlinear damping have also been studied in some articles. Ho et al. [145] studied the damping force in the form of $F_c = C_1\dot{x} + C_3x^3$ and its effect on the dynamic characteristics of the QZS isolator. They found that under force excitation, this type of damping, which belongs to the displacement-unrelated nonlinear viscous damping, can achieve a similar effect to the displacement-related hardening viscous damping, i.e. suppressing the transmissibility in the resonance region without affecting the high frequency transmissibility. Milovanovic et al. [146] found that under the base excitation that has a constant displacement amplitude for different frequencies, this type of damping could deteriorate the high frequency isolation performance. Wen et al. [147] studied the effect of shear-thinning viscous damping on the dynamic characteristics of the QZS isolator. The shear-thinning viscous damping is generated from non-Newtonian fluid, whose damping force satisfies the relationship of $F_c = \epsilon x^n$ ($n < 1$), thus belonging to displacement-unrelated nonlinear viscous damping. It was found that the conflict between the resonance region and high frequency region could not be resolved by designing the viscosity coefficient ϵ ; however, by reducing the flow index n , the resonant response could be greatly suppressed or even eliminated without affecting the high frequency transmissibility. Some researchers have also studied the utilization of nonlinear non-viscous damping for the performance enhancement of QZS isolators. For example, Liu et al. [148] and Donmez et al. [149] introduced dry friction damping into the QZS isolator in two different manners, and Hu et al. [150] connected the hysteresis damper in parallel with the oblique spring of the three-spring QZS isolator to produce nonlinear hysteresis damping characteristics; these nonlinear non-viscous damping characteristics can also enhance the isolation performance of QZS isolators to some extent by proper design of the damping parameters.

4.7. Active and semi-active controls

Active vibration control refers to the utilization of an active control algorithm to drive the actuator to exert a controllable force on the vibration control object according to the feedback vibration signal to achieve vibration suppression. Semi-active vibration control refers to the real-time control of some key system parameters (such as stiffness, damping, etc.) according to the detected vibration signal to suppress the undesirable vibration. Active and semi-active control methods are usually used in linear vibration isolation systems, while in recent years, some researchers have applied them to QZS vibration isolation systems.

4.7.1. Active control

Time delay is an inevitable feature in active control, but it can also be exploited to strengthen the control performance by proper design [151]. Sun et al. [152] introduced linear time-delayed active control into the spring-linkage type QZS isolator by using a servo motor to control the stiffness of the auxiliary spring, as shown in Fig. 25(a). The time-delayed

active control law is $k_3 = k_0 g(\hat{y}(t' - \tau) - \hat{y}(t'))$, where τ is the delay time. The notable feature of this control method is the effective suppression of the resonant response, and a larger delay time can result in a better suppression effect within a certain parameter range. In addition, this control method can augment the robustness of the system and the stability of the static equilibrium point and decrease the settling time of the transient response subject to an impact load. Moreover, the controlled stiffness and especially the introduced time delay could be designed deliberately so that undesirable bifurcation and chaotic behaviors can be avoided or greatly suppressed. Sun et al. also introduced time-delayed active control into a multi-directional QZS isolator [153], showing that the resonant frequency and damping characteristics in the vertical direction are mainly related to structural parameters, while those in the horizontal direction are mainly related to active control parameters. In contrast to Sun et al. who tended to suppress chaos, Li et al. [154] utilized time-delayed active control for chaotification of the QZS vibration system to activate the chaotic behavior. The main purpose of chaotification is to enhance the ability to reform the profile of the line spectra of vibration signals, rendering it easier to reconstruct continuous spectra and mask the extruded line spectra. This process is of great importance for hiding the spectrum features of vibration signals for concealment capability. Cheng et al. [155] introduced the displacement-velocity feedback control into a spring-linkage type QZS isolator with consideration of the time delay, as shown in Fig. 25(b). The results showed that the time delay mainly affects the stability of the controlled system and weakly influences the isolation performance and that the displacement-velocity feedback control can effectively suppress the vibration in the resonant region without affecting the high frequency isolation performance.

4.7.2. Semi-active control

Ma et al. [156] designed a semi-active QZS vibration isolator incorporating two electromagnetic negative stiffness mechanisms and an electrical eddy-current mechanism to provide damping, as shown in Fig. 26(a). In this isolator, negative stiffness is produced by the interaction between two stationary electromagnetic coils and a movable permanent magnet, and semi-active control is realized by regulating the electric current in the coils to tune the stiffness characteristics. Based on the same control principle, Chang et al. [157] designed a semi-active electromagnetic QZS dynamic vibration absorber using an electromagnetic coil and axially magnetized ring-shaped permanent magnets, as shown in Fig. 26(b). The absorption frequency (anti-resonant frequency) could be tuned between 3.86 Hz and 4.67 Hz in the experiment by adjusting the electric current. Liu et al. [158] designed a real-time semi-active electromagnetic QZS vibration isolator, in which the negative stiffness is produced by two electromagnets and a magneto-rheological elastomer, as shown in Fig. 26(c). The electric current in the electromagnetic coil can be regulated according to the feedback signal from the displacement sensor so as to achieve real-time control of the stiffness. The essential difference from Refs. [156, 157] is that a driving board was designed to automatically regulate the electric current according to the real-time signal feedback, whereas the electric current in

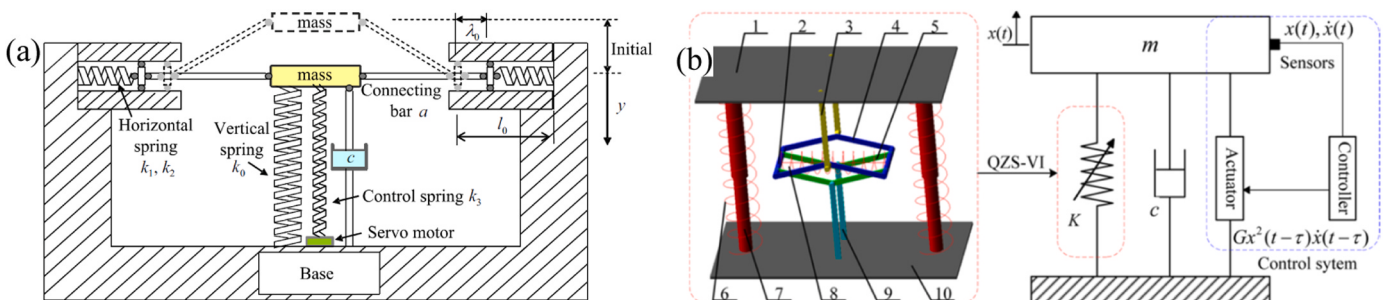


Fig. 25. QZS isolators with active control: (a) using time-delayed active control; (b) using displacement-velocity feedback control.

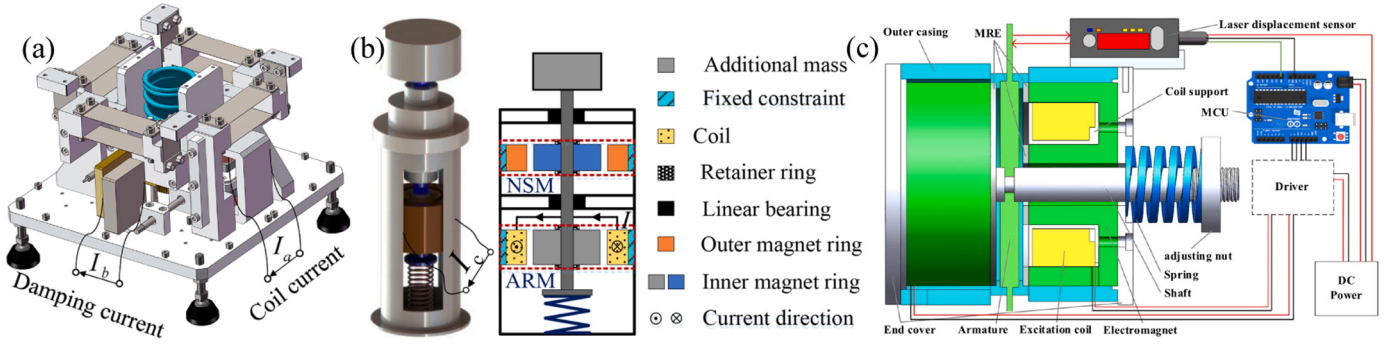


Fig. 26. QZS isolators with semi-active control: (a) semi-active electromagnetic QZS isolator; (b) semi-active electromagnetic QZS dynamic vibration absorber; (c) semi-active QZS isolator with real-time stiffness control using magnetorheological elastomer.

Refs.[156,157] is regulated manually. In addition to regulating the stiffness characteristics by controlling the electric current to realize semi-active vibration isolation, Wen et al. [159] proposed a semi-active QZS isolator by controlling the geometric relationship to regulate the stiffness characteristics, which is composed of six oblique springs and a vertical spring. The basic principle is to control the initial inclination angle of the oblique springs according to the displacement feedback signal for the modulation of stiffness characteristics. This semi-active control method renders the QZS isolator able to maintain good isolation performance under large excitation.

5. Applications

5.1. Applications in vehicles

For passenger cars, one of the most important considerations is the ride comfort of drivers and passengers. Spring-linkage type QZS isolators are usually utilized for the vibration isolation of vehicle seats to improve the ride comfort level. Le et al. [160] designed a vehicle seat as shown in Fig. 27(a) based on the spring-linkage type QZS vibration isolation model, which could produce a 67.2% reduction in the root-mean-square value of the displacement response under random excitation in the 0.1 Hz~10 Hz frequency band, whereas the linear isolator produced a 268.54% increase in the root-mean-square value of the displacement response, as shown in Fig. 27(b), which clearly indicates the excellent low-frequency vibration isolation performance of the spring-linkage type QZS vehicle seat. They also introduced a controllable pneumatic cylinder into the spring-linkage type QZS vehicle seat for active vibration control [161], as shown in Fig. 27(c). An adaptive intelligent backstepping controller was designed to manage the system operation, and an auxiliary control was also introduced to eliminate unfavorable effects caused by unpredictable perturbations. In addition, a radial basis function neural network model was utilized to estimate the optimal gain

of the auxiliary control effort. Liao et al. [162] applied the spring-linkage type QZS isolator with the nonlinear inerter shown in Fig. 17(a) to a vehicle seat, which could maintain good low-frequency vibration isolation performance under large excitation and small damping. The aforementioned studies on QZS vehicle seats only considered the vibration transmitted from the vehicle body to the seat, thus belonging to the SDOF vibration isolation problem. Wang et al. [163] examined the vibration isolation of vehicle seats from a more global perspective, and established a MDOF coupling model that includes road surface, wheel, vehicle body and seat, as shown in Fig. 27(d). The unevenness of the road surface causes basic excitation to the system. The coupling between the road surface and wheel and the coupling between the wheel and vehicle body are abstracted as the parallel combination of spring and damping. The spring-linkage type QZS isolator is employed between the vehicle body and the seat. This model considers the variable mass of the passengers and sets the total mass of the vehicle seat and human body as an uncertain parameter, thereby being able to investigate the overload and unload conditions in practical engineering. A constrained adaptive backstepping controller law based on the barrier Lyapunov function is utilized in this model to further improve the isolation performance. The results indicated that the designed controller law can isolate the shock excitation transmitted from the road to the passengers effectively, and both the vehicle and seat suspension strokes remain in allowed stroke range.

QZS isolators have also been applied in large-scale vehicle-mounted equipment and commercial vehicles. Chen et al. [164] applied the three-spring QZS isolator to a large-scale vehicle-mounted optic-electronic device, which achieved effective vibration isolation for the photoelectric device above 20 Hz and above 90% under complex road conditions, providing a solid foundation for the high-precision tracking of vehicle-mounted photoelectric devices. Commercial vehicles are carriers that drive long-term in complex and changing road interaction environments, especially trucks and mining vehicles.

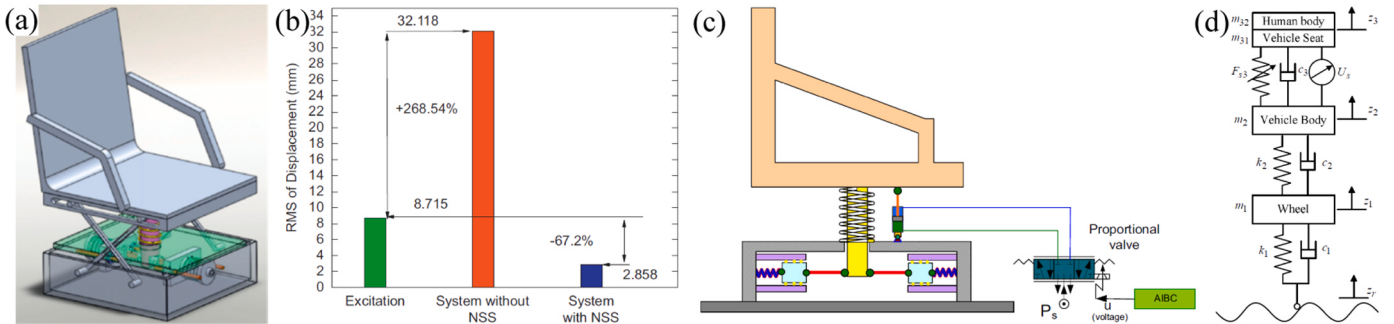


Fig. 27. Application of QZS isolators to vehicle seats: (a) structural diagram of a spring-linkage type QZS seat; (b) comparison of the isolation performance under low-frequency random excitation; (c) QZS vehicle seat with adaptive intelligent backstepping control; (d) coupling model of the wheel, vehicle body and vehicle seat with active control.

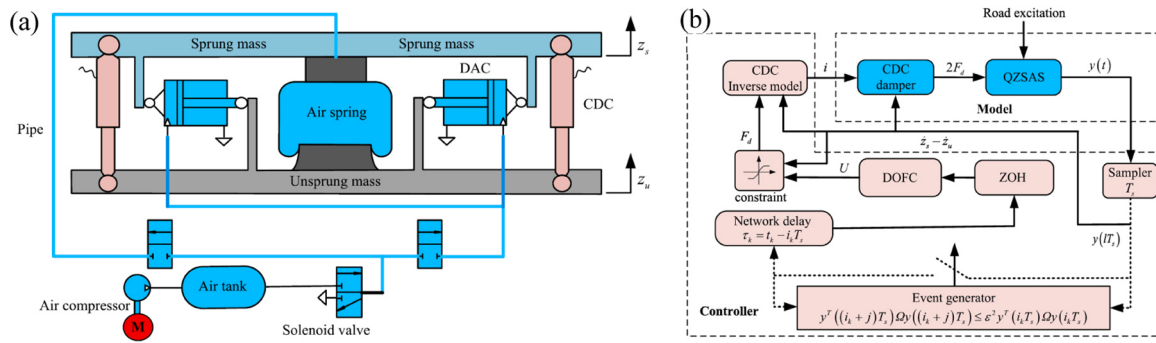


Fig. 28. Semi-active QZS air suspension for commercial vehicles: (a) schematic configuration; (b) network communication scheme of event trigger control.

Whether they can provide superior vibration isolation performance will directly affect the health of drivers and passengers and the safety of transported goods. Xu et al. [165] proposed a novel configuration of semi-active QZS air suspension with a network communication architecture, accompanied by a matching dynamic output feedback control strategy considering event-triggered mechanism. The semi-active QZS air suspension is mainly composed of a positive stiffness air spring, a pair of negative stiffness double-acting cylinders (DACs) and two continuous damping-controlled (CDC) dampers, as shown in Fig. 28(a). The event-triggered mechanism determines whether the control signal is updated by judging the measured signal to save communication resources, as shown in Fig. 28(b). The nonlinear stiffness of the suspension system is regarded as an uncertain parameter and processed by constructing a Takagi-Sugeno fuzzy controller model. The Lyapunov-Krasovskii functional method is employed to design the dynamic output feedback controller under the linear matrix inequality constraint to ensure system stability with the H_∞ performance index. The co-simulation and hardware-in-the-loop test results indicated that the proposed semi-active QZS air suspension and the H_∞ dynamic output feedback control method with event-triggered mechanism can significantly improve the multi-objective performance of commercial vehicles under different driving conditions with a very small network communication burden.

5.2. Applications in civil engineering

Vibration suppression of bridge is an important issue in civil engineering, since excessive vibration of bridge will cause not only the damage of bridge itself but also the unsafety of vehicles and people travelling through it. Bouna et al. [166] considered a vibration control problem for a multi-span continuous bridge under pier base vibrating excitation by utilizing multiple QZS isolators. Each of the QZS isolators is placed between a pier and the bridge structure to collaboratively isolate the vibration of the bridge, as shown in Fig. 29(a). Results show that the QZS isolator with suitable parameters has the advantage of more effectively isolating unwanted vibrations transmitted from the

foundation to the bridge, as it can achieve excellent low-frequency isolation performance including low initial isolation frequency and wide isolation frequency band. They have also studied the performance of the multi-span continuous bridge supported by multiple QZS isolators in the presence of a moving mass [167], to mimic a car traveling on the bridge. Results indicate that the mounted multiple QZS isolators can still effectively suppress the vibration of the bridge even if there is a moving mass on it. Attary et al. [168] designed a QZS seismic response control device for highway bridge subjected to various strong earthquake ground motions, as shown in Fig. 29(b), which is composed of a negative stiffness structure in parallel with a positive stiffness structure. They have also conducted the shake table testing, revealing that the use of such a device in a seismically isolated bridge can significantly reduce the peak base shear [169].

Earthquakes usually bring powerful shocks and vibrations, posing serious threat to houses, buildings and human safety. Many seismic isolation devices are designed to protect structures from the strong horizontal component of earthquake ground shaking [170]. As the structure needs to maintain its load bearing capacity, using the horizontal isolation strategy in vertical seismic isolation will lead to the problem of larger static displacement. However, in near-fault seismic zones, the vertical acceleration experienced during a strong earthquake can be greater than the horizontal acceleration, which actually deserves more attention in anti-seismic design. The QZS vibration isolation technology provides an effective solution for this issue [171]. Liu et al. [172] utilized the three-spring QZS vibration isolation model to design a vertical anti-seismic system to protect the structures subjected to near-fault vertical earthquakes. Results show that the seismic response of the structure can be controlled by setting appropriate static equilibrium position, vertical isolation period and vertical damping ratio. Eskandary et al. [173] employed the spring-linkage QZS isolation model to develop a vertical anti-seismic structure and used eight scaled real earthquake excitation signals for experimental verification. Results show that the designed anti-seismic structure can significantly reduce the transmission of acceleration and force, with seven of the eight earthquake inputs exhibiting good performance. One exception is the

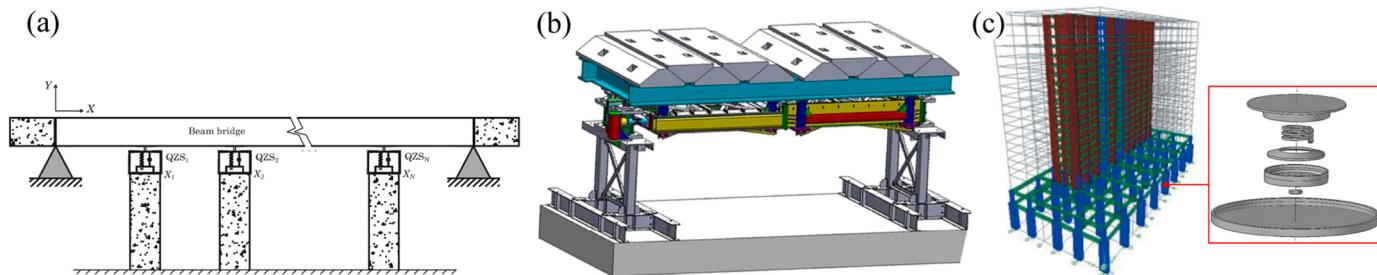


Fig. 29. Applications of QZS isolation method in civil engineering: (a) multi-span continuous bridge supported by multiple QZS isolators; (b) QZS anti-seismic device for highway bridge; (c) QZS anti-seismic design for tall building.

Chi-Chi earthquake signal, but numerical results show that the Chi-Chi earthquake can also be suppressed by changing the design parameters of the QZS anti-seismic structure. Li et al. [174] introduced active control into a QZS seismic protection structure to adapt to various earthquakes. Three representative control algorithms, i.e. linear quadratic regular (LQR) control, H_{oo} control and sliding mode (SM) control, are utilized to attain optimal control force. Four scaled benchmark earthquakes are employed as excitations for the case study. Results show that, in addition to good suppression effect on peak floor displacement and peak inter-storey drift, the QZS seismic protection structure with active control also achieves superior performance on mitigating peak structure shear and peak acceleration response of the first floor. Cimellaro et al. [175] designed a three-directional QZS seismic isolation system to control both the horizontal and vertical components of ground motion in strong earthquakes. A set of earthquake records typical of the near-fault regions with the characteristic of pulse shape were selected to perform the nonlinear dynamic analyses. Simulation results show good anti-seismic performance in three directions especially in the vertical direction. Zhou et al. [176] focused on the seismic protection of buildings subjected to earthquakes. They designed a novel three-dimensional seismic isolator combining the QZS system in the vertical direction and the friction pendulum system in the horizontal direction [177] and applied it to a tall building, as shown in Fig. 29(c). Results indicate that the overturning movement can be controlled within safe limit under maximum considered earthquake, and the human discomfort from high frequency environment vibration can be significantly decreased.

5.3. Other applications

Ding et al. [178] employed two three-spring isolators to support the fluid-conveying pipe to attenuate its transverse vibration induced by foundation excitation, as shown in Fig. 30(a). They established a dynamic model of nonlinear forced vibration for the fluid-conveying pipe coupled with two QZS isolators and validated it by using the Galerkin method and finite difference method. The results showed that effective vibration isolation can be achieved at high frequencies, the maximum resonant peak can be shifted to low-frequency region, and the bending vibration of the pipe in the low-frequency region can be reduced; however, several low-order vibration modes may also move to low-frequency region, and the rigid body motion of the pipe in the low-frequency region is large, bringing new challenges to the vibration isolation of continuous systems. Zhou et al. [179] applied QZS vibration isolation technology to an incubator during neonatal transport, as shown in Fig. 30(b). The infant housing unit is supported by four QZS isolators to mitigate mechanical vibration being transmitted from the ambulance floor to the infant. Each of the QZS isolators was devised by combining a pair of permanent ring-shaped magnets and a coil spring. The RMS value of the acceleration response of the infant model in the housing unit is reduced to 32.3% under random excitation in the 2 Hz–15 Hz frequency band. They have also established a coupled lumped parameter model incorporating the ambulance floor, wheels, auxiliary equipment, QZS isolators, infant compartment, mattress and infant [180], revealing that a relatively large damping is needed to

completely eliminate the jump phenomenon and suppress resonance so as to ensure an ultra-low beginning frequency of vibration isolation. Jing et al. [181] applied the scissor-like structure with QZS feature to a hand-held jackhammer, as shown in Fig. 30(c). This structure could greatly reduce the dynamic load of the reaction force on the palms of operators in the process of demolition, thus being of great significance to the health protection of demolition operators and higher demolition efficiency.

6. Conclusions and future prospects

The QZS vibration isolation technology breaks through the conflict between low dynamic stiffness and high static stiffness, which can thus extend the vibration isolation band to low frequency region, providing an effective solution to low frequency vibration isolation problems in mechanical engineering, civil engineering, aerospace engineering, vehicle engineering, transportation engineering, instrument engineering, etc. In this paper, the research progress of QZS vibration isolation technology in recent decades is reviewed, with the designs and the improvement strategies being emphasized. There are three main categories of approaches for constructing QZS isolators, i.e. the geometric nonlinearity, the magnetic nonlinearity and the exploitation of deformable components. These approaches can produce negative stiffness by their respective nonlinear mechanisms, and the QZS property is obtained by connecting negative and positive stiffness elements in parallel with well-chosen parameters. Many improvement strategies are expounded in detail in this paper to further enhance the overall performance of QZS isolators from various aspects, including broadening the low-stiffness displacement range, nonlinear compensation method, designs for supporting different loads, suppressing the rightward bending of resonance region, increasing the roll-off rate in high frequency region, introducing nonlinear damping, and introducing active and semi-active controls. Some application examples of QZS isolators in engineering are also described in this paper. It should be noted that this paper is not intended to compare the performances of different QZS isolators constructed by various design approaches, whereas the aim of this paper is to provide a comprehensive overview of the QZS vibration isolation technology for researchers in related fields. Despite the tremendous research achievements on QZS vibration isolation, there still remain a few issues needing to be resolved, and QZS vibration isolation technology can also be further developed by integrating new ideas. Therefore, future research on QZS vibration isolation can evolve in the following directions:

(1) Accurate modelling of QZS isolators

The issue of inaccurate modelling exists widely in previous studies on QZS isolators, which is reflected in three main aspects. The first is the neglect of the masses of components and the damping generation sources (for example, the friction in revolution joint) when formulating the dynamic equation(s). However, the component masses and the damping generation sources can inevitably affect the inertial characteristics and the damping characteristics respectively of the whole system and thus have significant influences on the dynamic behaviors. Secondly, the

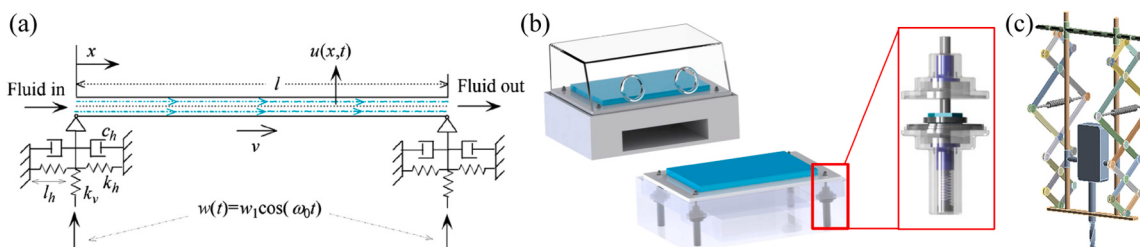


Fig. 30. Other applications of QZS isolators: (a) fluid-conveying pipe; (b) incubator for neonatal transport; (c) hand-held jackhammer.

restoring force term is usually approximated by a polynomial for simpler analytical calculation of the dynamic response, which causes inaccuracy again. Thirdly, 6DOF QZS vibration isolation platforms are usually modelled with ignoring the nonlinear coupled terms and retaining the nonlinear uncoupled terms to analyze each DOF separately. All three kinds of inaccuracy lead to inaccurate theoretical results and make it impossible to manifest the essential dynamic characteristics. Consequently, it should be explored to establish accurate dynamic models for the QZS isolators with consideration of practical factors and to study the dynamic characteristics without polynomial approximation. It is also necessary to study the effects of nonlinear coupling on the dynamic behaviors of the 6DOF QZS isolation platform as a high-dimensional nonlinear system and to reduce the degree of nonlinear coupling through structural optimization design.

(2) Design for higher robustness and reliability

As nonlinear systems, most QZS isolators are usually sensitive to parameter uncertainties, which may lead to unexpected dynamic behaviors under non-ideal conditions. For this reason, the QZS isolators may not achieve the anticipated vibration isolation performance or may even be counterproductive under extreme external conditions that exist widely in engineering, resulting in poor robustness. Besides, the QZS isolators are generally more complicated than linear isolators in terms of structural composition, leading to larger size and weight, which also hinders the engineering application. In addition, the application of QZS isolators may involve multi-physical fields with thermal, acoustic, electrical and magnetic coupling, thus requiring a high reliability. Consequently, it is a meaningful and challenging task to design QZS isolators with high robustness and reliability for engineering applications. It is also interesting to integrate the QZS vibration isolation philosophy into the engineering structure itself for higher robustness and reliability instead of inserting an additional system, i.e. the modification or reconfiguration of the engineering structure to enable inherent QZS property for robust, reliable and high-efficiency vibration isolation.

(3) Synergistic design of QZS vibration isolation and energy harvesting

From the perspective of energy flow, vibration isolation implies inhibiting the transfer of mechanical energy to vibration isolation object. Therefore, it is feasible to incorporate electromagnetic, piezoelectric, triboelectric and other energy conversion elements into the QZS structure to convert part of the vibration energy into other forms in the vibration transmission path and meanwhile reduce the vibration energy flowing to the isolation object, thereby achieving simultaneous low-frequency vibration isolation and energy harvesting. The emphasis is placed on how to integrate the two objectives and benefit each other with a synergistic effect, which needs to resort to nonlinear targeted energy transfer mechanism. The synergistic design of QZS vibration isolation and energy harvesting can be applied to engineering systems that require both low-frequency vibration suppression of core components and low power supply to maintain normal operation. The harvested energy can also be exploited to supply the system itself for self-powered semi-active vibration control.

(4) Data-driven-based intelligent control of QZS isolation systems

Traditionally, vibration control relied on predetermined control strategies that lacked adaptability and real-time responsiveness. With the advent of data-driven-based intelligent control, the control system can dynamically analyze and process vast amounts of data collected from sensors, enabling it to make informed decisions and adjust its control parameters accordingly. Therefore the introduction of data-driven-based intelligent control into QZS vibration isolation systems will be a promising trend. To fully harness the potential of data-driven-

based intelligent control for QZS vibration isolation systems, future works may include the following: (a) Integration with advanced sensor technologies: Incorporating emerging sensor technologies, such as wireless sensor networks and Internet of Things (IoT) devices, can enhance data collection capabilities and enable real-time control. (b) Hybrid control approaches: Combining data-driven techniques with model-based control approaches can leverage the strengths of both paradigms, improving control accuracy and adaptability. (c) Model interpretability: Since the black-box nature of some data-driven techniques may hinder the interpretability of control decisions, developing transparent models and explainable artificial intelligence methods is essential for practical implementation.

CRediT authorship contribution statement

Zhang Wei: Supervision. **Yu Kaiping:** Supervision. **Liu Tao:** Visualization. **Zheng Yan:** Visualization. **Liu Chaoran:** Writing – review & editing, Writing – original draft, Visualization, Validation, Software, Resources, Project administration, Methodology, Investigation, Funding acquisition, Formal analysis, Data curation, Conceptualization.

Declaration of Competing Interest

The authors declare that they have no known competing financial interests or personal relationships that could have appeared to influence the work reported in this paper.

Data Availability

The data that has been used is confidential.

Acknowledgements

The authors would like to acknowledge the support of the National Natural Science Foundation of China (Grant Nos. 12302002 and 11832002) and the Beijing Postdoctoral Research Foundation (Grant No. 2023-zz-80).

References

- [1] Sheng T, Liu GB, Bian XC, et al. Development of a three-directional vibration isolator for buildings subject to metro- and earthquake-induced vibrations. *Eng Struct* 2022;252:113576.
- [2] Ismail M. Inner pounding control of the RNC isolator and its impact on seismic isolation efficiency under near-fault earthquakes. *Eng Struct* 2015;86:99–121.
- [3] Liu C, Jing X, Daley S, et al. Recent advances in micro-vibration isolation. *Mech Syst Signal Process* 2015;56–57:55–80.
- [4] Song G, Sethi V, Li HN. Vibration control of civil structures using piezoceramic smart materials: A review. *Eng Struct* 2006;28:1513–24.
- [5] Lu Z, Zhao S, Ma C, et al. Experimental and analytical study on the performance of wind turbine tower attached with particle tuned mass damper. *Eng Struct* 2023;294:116784.
- [6] Li H, Li Y, Li J. Negative stiffness devices for vibration isolation applications: A review. *Adv Struct Eng* 2020;23:1739–55.
- [7] Ibrahim RA. Recent advances in nonlinear passive vibration isolators. *J Sound Vib* 2008;314:371–452.
- [8] Ma Z, Zhou R, Yang Q. Recent Advances in Quasi-Zero Stiffness Vibration Isolation Systems: An Overview and Future Possibilities. *Machines* 2022;10:813.
- [9] Ding H, Chen LQ. Designs, analysis, and applications of nonlinear energy sinks. *Nonlinear Dyn* 2020;100:3061–107.
- [10] Saeed AS, Nasar RA, AL-Shudeifat MA. A review on nonlinear energy sinks: designs, analysis and applications of impact and rotary types. *Nonlinear Dyn* 2023;111:1–37.
- [11] Zhang Y, Cao Q. The recent advances for an archetypal smooth and discontinuous oscillator. *Int J Mech Sci* 2022;214:106904.
- [12] Carrella A, Brennan MJ, Waters TP. Optimization of a Quasi-Zero-Stiffness Isolator. *J Mech Sci Technol* 2007;21:946–9.
- [13] Carrella A, Brennan MJ, Kovacic I, et al. On the force transmissibility of a vibration isolator with quasi-zero-stiffness. *J Sound Vib* 2009;322:707–17.
- [14] Carrella A, Brennan MJ, Waters TP. Static analysis of a passive vibration isolator with quasi-zero-stiffness characteristic. *J Sound Vib* 2007;301:678–89.
- [15] Zhang Y, Cao Q, Huang W. Bursting oscillations in an isolation system with quasi-zero stiffness. *Mech Syst Signal Process* 2021;161:107916.

- [16] Hao Z, Cao Q, Wiercigroch M. Nonlinear dynamics of the quasi-zero-stiffness SD oscillator based upon the local and global bifurcation analyses. *Nonlinear Dyn* 2017;87:987–1014.
- [17] Liu C, Yu K. Accurate modeling and analysis of a typical nonlinear vibration isolator with quasi-zero stiffness. *Nonlinear Dyn* 2020;100:2141–65.
- [18] Lan CC, Yang SA, Wu YS. Design and experiment of a compact quasi-zero-stiffness isolator capable of a wide range of loads. *J Sound Vib* 2014;333:4843–58.
- [19] Tian Y, Cao D, Chen C, et al. Vibration isolation performance of a rectangular panel with high-static-low-dynamic stiffness supports. *Appl Math Model* 2023;219:218–38.
- [20] Xu D, Zhang Y, Zhou J, et al. On the analytical and experimental assessment of the performance of a quasi-zero-stiffness isolator. *J Vib Control* 2013;20:2314–25.
- [21] Liu C, Yu K. Design and experimental study of a quasi-zero-stiffness vibration isolator incorporating transverse groove springs. *Arch Civ Mech Eng* 2020;20:67.
- [22] Le TD, Ahn KK. Experimental investigation of a vibration isolation system using negative stiffness structure. *Int J Mech Sci* 2013;70:99–112.
- [23] Wang X, Liu H, Chen Y, et al. Beneficial stiffness design of a high-static-low-dynamic-stiffness vibration isolator based on static and dynamic analysis. *Int J Mech Sci* 2018;142–143:235–44.
- [24] Liu C, Yu K. Superharmonic resonance of the quasi-zero-stiffness vibration isolator and its effect on the isolation performance. *Nonlinear Dyn* 2020;100:95–117.
- [25] Zhou J, Wang X, Xu D, et al. Nonlinear dynamic characteristics of a quasi-zero stiffness vibration isolator with cam-roller-spring mechanisms. *J Sound Vib* 2015;346:53–69.
- [26] Zhou J, Xu D, Bishop S. A torsion quasi-zero stiffness vibration isolator. *J Sound Vib* 2015;338:121–33.
- [27] Wang K, Zhou J, Xu D. Sensitivity analysis of parametric errors on the performance of a torsion quasi-zero-stiffness vibration isolator. *Int J Mech Sci* 2017;134:336–46.
- [28] Sun X, Jing X, Xu J, et al. Vibration isolation via a scissor-like structured platform. *J Sound Vib* 2014;333:2404–20.
- [29] Bian J, Jing X. Analysis and design of a novel and compact X-structured vibration isolation mount (X-Mount) with wider quasi-zero-stiffness range. *Nonlinear Dyn* 2020;101:2195–222.
- [30] Chai Y, Jing X, Chao X. X-shaped mechanism based enhanced tunable QZS property for passive vibration isolation. *Int J Mech Sci* 2022;218:107077.
- [31] Sun X, Jing X. Analysis and design of a nonlinear stiffness and damping system with a scissor-like structure. *Mech Syst Signal Process* 2016;66–67:723–42.
- [32] Jing X, Zhang L, Jiang G, et al. Critical factors in designing a class of X-shaped structures for vibration isolation. *Eng Struct* 2019;199:109659.
- [33] Han H, Sorokin V, Tang L, et al. A nonlinear vibration isolator with quasi-zero-stiffness inspired by Miura-origami tube. *Nonlinear Dyn* 2021;105:1313–25.
- [34] Ye K, Ji JC. An origami inspired quasi-zero stiffness vibration isolator using a novel truss-spring based stack Miura-ori structure. *Mech Syst Signal Process* 2022;165:108383.
- [35] Feng X, Jing X, Xu Z, et al. Bio-inspired anti-vibration with nonlinear inertia coupling. *Mech Syst Signal Process* 2019;124:562–95.
- [36] Zeng R, Wen G, Zhou J, et al. Limb-inspired bionic quasi-zero stiffness vibration isolator. *Acta Mech Sin* 2021;37:1152–67.
- [37] Ling P, Miao L, Zhang W, et al. Cockroach-inspired structure for low-frequency vibration isolation. *Mech Syst Signal Process* 2022;171:108955.
- [38] Ling P, Miao L, Ye B, et al. Ultra-low frequency vibration isolation of a novel click-beetle-inspired structure with large quasi-zero stiffness region. *J Sound Vib* 2023;558:117756.
- [39] Wang J, Wierschem N, Spencer BF, et al. Experimental study of track nonlinear energy sinks for dynamic response reduction. *Eng Struct* 2015;94:9–15.
- [40] Dou J, Yao H, Li H, et al. A track nonlinear energy sink with restricted motion for rotor systems. *Int J Mech Sci* 2023;259:108631.
- [41] Virgin LN, Davis RB. Vibration isolation using buckled struts. *J Sound Vib* 2003;260:965–73.
- [42] Liu X, Huang X, Hua H. On the characteristics of a quasi-zero stiffness isolator using Euler buckled beam as negative stiffness corrector. *J Sound Vib* 2013;332:3359–76.
- [43] Huang X, Liu X, Sun J, et al. Vibration isolation characteristics of a nonlinear isolator using Euler buckled beam as negative stiffness corrector: A theoretical and experimental study. *J Sound Vib* 2014;333:1132–48.
- [44] Huang X, Liu X, Sun J, et al. Effect of the system imperfections on the dynamic response of a high-static-low-dynamic stiffness vibration isolator. *Nonlinear Dyn* 2014;76:1157–67.
- [45] Chen R, Li X, Yang Z, et al. A variable positive-negative stiffness joint with low frequency vibration isolation performance. *Measurement* 2021;185:110046.
- [46] Liu C, Zhao R, Yu K, et al. A quasi-zero-stiffness device capable of vibration isolation and energy harvesting using piezoelectric buckled beams. *Energy* 2021;233:121146.
- [47] Zhang C, He J, Zhou G, et al. Compliant quasi-zero-stiffness isolator for low-frequency torsional vibration isolation. *Mech Mach Theory* 2023;181:105213.
- [48] Fulcher BA, Shahan DW, Haberman MR, et al. Analytical and Experimental Investigation of Buckled Beams as Negative Stiffness Elements for Passive Vibration and Shock Isolation Systems. *J Vib Acoust* 2014;136:031009.
- [49] Lian X, Deng H, Han G, et al. A low-frequency micro-vibration absorber based on a designable quasi-zero stiffness beam. *Aerospace Sci Technol* 2023;132:108044.
- [50] Kocak K, Yilmaz G. Design of a compliant lever-type passive vibration isolator with quasi-zero-stiffness mechanism. *J Sound Vib* 2023;558:117758.
- [51] Dalela S, Balaji PS, Jena DP. Design of a metastructure for vibration isolation with quasi-zero-stiffness characteristics using bistable curved beam. *Nonlinear Dyn* 2022;108:1931–71.
- [52] Cai C, Zhou JX, Wu L, et al. Design and numerical validation of quasi-zero-stiffness metamaterials for very low-frequency band gaps. *Compos Struct* 2020;236:111862.
- [53] Fan H, Yang L, Tian Y, et al. Design of metastructures with quasi-zero dynamic stiffness for vibration isolation. *Compos Struct* 2020;243:112244.
- [54] Huang X, Liu X, Hua H. On the characteristics of an ultra-low frequency nonlinear isolator using sliding beam as negative stiffness. *J Mech Sci Technol* 2014;28:813–22.
- [55] Ibrahim RA. Recent advances in nonlinear passive vibration isolators. *J Sound Vib* 2008;314:371–452.
- [56] Ibrahim RA, Somnay RJ. Nonlinear dynamic analysis of an elastic beam isolator sliding on frictional supports. *J Sound Vib* 2007;308:735–57.
- [57] Qi WH, Yan G, Lu JJ, et al. Magnetically modulated sliding structure for low frequency vibration isolation. *J Sound Vib* 2022;526:116819.
- [58] Hyer MW. Calculations of the room-temperature shapes of unsymmetric laminates. *J Compos Mater* 1981;15:296–310.
- [59] Shaw AD, Neild SA, Wagg DJ, et al. A nonlinear spring mechanism incorporating a bistable composite plate for vibration isolation. *J Sound Vib* 2013;332:6265–75.
- [60] Li M, Li Y, Liu X, et al. A quasi-zero-stiffness vibration isolator using bi-stable hybrid symmetric laminate. *Compos Struct* 2022;299:116047.
- [61] Liu S, Peng G, Jin K. Design and characteristics of a novel QZS vibration isolation system with origami-inspired corrector. *Nonlinear Dyn* 2021;106:255–77.
- [62] Liu S, Peng G, Jin K. Towards accurate modeling of the Tachi-Miura origami in vibration isolation platform with geometric nonlinear stiffness and damping. *Appl Math Model* 2022;103:674–95.
- [63] Sadeghi S, Li S. Fluidic origami cellular structure with asymmetric quasi-zero stiffness for low-frequency vibration isolation. *Smart Mater Struct* 2019;28:065006.
- [64] Ishida S, Uchida H, Shimosaka H, et al. Design and Numerical Analysis of Vibration Isolators With Quasi-Zero-Stiffness Characteristics Using Bistable Foldable Structures. *J Vib Acoust* 2017;139:031015.
- [65] Ishida S, Suzuki K, Shimosaka H. Design and Experimental Analysis of Origami-Inspired Vibration Isolator With Quasi-Zero-Stiffness Characteristic. *J Vib Acoust* 2017;139:051004.
- [66] Han H, Sorokin V, Tang L, et al. Lightweight origami isolators with deployable mechanism and quasi-zero-stiffness property. *Aerospace Sci Technol* 2022;121:107319.
- [67] Xu D, Yu Q, Zhou J, et al. Theoretical and experimental analyses of a nonlinear magnetic vibration isolator with quasi-zero-stiffness characteristic. *J Sound Vib* 2013;332:3377–89.
- [68] Su P, Wu J, Liu S, et al. A study of a nonlinear magnetic vibration isolator with quasi-zero-stiffness. *J Vibroengineering* 2018;20:310–20.
- [69] Jiang Y, Song C, Ding C, et al. Design of magnetic-air hybrid quasi-zero stiffness vibration isolation system. *J Sound Vib* 2020;477:115346.
- [70] Zhou N, Liu K. A tunable high-static-low-dynamic stiffness vibration isolator. *J Sound Vib* 2010;329:1254–73.
- [71] Carrella A, Brennan MJ, Waters TP, et al. On the design of a high-static-low-dynamic stiffness isolator using linear mechanical springs and magnets. *J Sound Vib* 2008;315:712–20.
- [72] Robertson WS, Kidner MRF, Cazzolato BS, et al. Theoretical design parameters for a quasi-zero stiffness magnetic spring for vibration isolation. *J Sound Vib* 2009;326:88–103.
- [73] Wu W, Chen X, Shan Y. Analysis and experiment of a vibration isolator using a novel magnetic spring with negative stiffness. *J Sound Vib* 2014;333:2958–70.
- [74] Sun X, Wang F, Xu J. Analysis, design and experiment of continuous isolation structure with Local Quasi-Zero-Stiffness property by magnetic interaction. *Int J Non-Linear Mech* 2019;116:289–301.
- [75] Wu J, Zeng L, Han B, et al. Analysis and design of a novel arrayed magnetic spring with high negative stiffness for low-frequency vibration isolation. *Int J Mech Sci* 2022;216:106980.
- [76] Zheng Y, Zhang X, Luo Y, et al. Design and experiment of a high-static-low-dynamic stiffness isolator using a negative stiffness magnetic spring. *J Sound Vib* 2016;360:31–52.
- [77] Zheng Y, Zhang X, Luo Y. Analytical study of a quasi-zero stiffness coupling using a torsion magnetic spring with negative stiffness. *Mech Syst Signal Process* 2018;100:135–51.
- [78] Xu J, Yang X, Li W, et al. Design of quasi-zero stiffness joint actuator and research on vibration isolation performance. *J Sound Vib* 2020;479:115367.
- [79] Dong G, Zhang X, Xie S, et al. Simulated and experimental studies on a high-static-low-dynamic stiffness isolator using magnetic negative stiffness spring. *Mech Syst Signal Process* 2017;86:188–203.
- [80] Wang Q, Zhou J, Wang K, et al. Design and experimental study of a compact quasi-zero-stiffness isolator using wave springs. *Sci China Technol Sci* 2021;64:2255–71.
- [81] Yan B, Yu N, Wang Z, et al. Lever-type quasi-zero stiffness vibration isolator with magnetic spring. *J Sound Vib* 2022;527:116865.
- [82] Palomares E, Nieto AJ, Morales AL, et al. Numerical and experimental analysis of a vibration isolator equipped with a negative stiffness system. *J Sound Vib* 2017;414:31–42.
- [83] An J, Chen G, Deng X, et al. Analytical study of a pneumatic quasi-zero-stiffness isolator with mistuned mass. *Nonlinear Dyn* 2022;108:3297–312.
- [84] Vo NYP, Le TD. Adaptive pneumatic vibration isolation platform. *Mech Syst Signal Process* 2019;133:106258.

- [85] Meng L, Sun J, Wu W. Theoretical design and characteristics analysis of a quasi-zero stiffness isolator using a disk spring as negative stiffness element. *Shock Vib* 2015;2015:813763.
- [86] Chen P, Wang B, Zhou D, et al. Performance evaluation of a nonlinear energy sink with quasi-zero stiffness property for vertical vibration control. *Eng Struct* 2023; 282:115801.
- [87] Gao X, Chen Q. Static and dynamic analysis of a high static and low dynamic stiffness vibration isolator utilising the solid and liquid mixture. *Eng Struct* 2015; 99:205–13.
- [88] Liu C, Zhao R, Yu K, et al. In-plane quasi-zero-stiffness vibration isolator using magnetic interaction and cables: Theoretical and experimental study. *Appl Math Model* 2021;96:497–522.
- [89] Sun X, Jing X. A nonlinear vibration isolator achieving high-static-low-dynamic stiffness and tunable anti-resonance frequency band. *Mech Syst Signal Process* 2016;80:166–88.
- [90] Zhang Q, Xie S, Xu D, et al. A torsion-translational vibration isolator with quasi-zero stiffness. *Nonlinear Dyn* 2020;99:1467–88.
- [91] Ye K, Ji JC, Brown T. A novel integrated quasi-zero stiffness vibration isolator for coupled translational and rotational vibrations. *Mech Syst Signal Process* 2021; 149:107340.
- [92] Chai Y, Jing X, Guo Y. A compact X-shaped mechanism based 3-DOF anti-vibration unit with enhanced tunable QZS property. *Mech Syst Signal Process* 2022;168:108651.
- [93] Chai Y, Jing X. Low-frequency multi-direction vibration isolation via a new arrangement of the X-shaped linkage mechanism. *Nonlinear Dyn* 2022;109: 2383–421.
- [94] Dong G, Zhang X, Luo Y, et al. Analytical study of the low frequency multi-direction isolator with high-static-low-dynamic stiffness struts and spatial pendulum. *Mech Syst Signal Process* 2018;110:521–39.
- [95] Tu J, Deng Z, Huang W, et al. A six degree of freedom passive vibration isolator with quasi-zero-stiffness-based supporting. *J Low Freq Noise, Vib Act Control* 2018;37:279–94.
- [96] Yang T, Cao Q. Modeling and analysis of a novel multi-directional micro-vibration isolator with spring suspension struts. *Arch Appl Mech* 2022;92: 801–19.
- [97] Liu C, Yu K, Pang S. A novel eight-legged vibration isolation platform with dual-pyramid-shape struts. *Meccanica* 2019;54:873–99.
- [98] Zhou J, Xiao Q, Xu D, et al. A novel quasi-zero-stiffness strut and its applications in six-degree-of-freedom vibration isolation platform. *J Sound Vib* 2017;394: 59–74.
- [99] Liu Y, Ji W, Gu H, et al. Force transmissibility of a 6-DOF passive quasi-zero stiffness vibration isolation platform. *J Mech Sci Technol* 2021;35:2313–24.
- [100] Zhou J, Wang K, Xu D, et al. A Six Degrees-of-Freedom Vibration Isolation Platform Supported by a Hexapod of Quasi-Zero-Stiffness Struts. *J Vib Acoust* 2017;139:034502.
- [101] Zheng Y, Li Q, Yan B, et al. A Stewart isolator with high-static-low-dynamic stiffness struts based on negative stiffness magnetic springs. *J Sound Vib* 2018; 422:390–408.
- [102] Zhao F, Ji J, Ye K, et al. Increase of quasi-zero stiffness region using two pairs of oblique springs. *Mech Syst Signal Process* 2020;144:106975.
- [103] Zhao F, Cao S, Luo Q, et al. Enhanced design of the quasi-zero stiffness vibration isolator with three pairs of oblique springs: Theory and experiment. *J Vib Control* 2022.
- [104] Zhao F, Ji J, Luo Q, et al. An improved quasi-zero stiffness isolator with two pairs of oblique springs to increase isolation frequency band. *Nonlinear Dyn* 2021;104: 349–65.
- [105] Yang T, Cao Q, Hao Z. A novel nonlinear mechanical oscillator and its application in vibration isolation and energy harvesting. *Mech Syst Signal Process* 2021;155: 107636.
- [106] Zhao F, Ji J, Ye K, et al. An innovative quasi-zero stiffness isolator with three pairs of oblique springs. *Int J Mech Sci* 2021;192:106093.
- [107] Gatti G, Ledezma-Ramirez DF, Brennan MJ. Performance of a shock isolator inspired by skeletal muscles. *Int J Mech Sci* 2023;244:108066.
- [108] Chen T, Zheng Y, Song L, et al. Design of a new quasi-zero-stiffness isolator system with nonlinear positive stiffness configuration and its novel features. *Nonlinear Dyn* 2023;111:5141–63.
- [109] Zuo S, Wang D, Zhang Y, et al. Design and testing of a parabolic cam-roller quasi-zero-stiffness vibration isolator. *Int J Mech Sci* 2022;220:107146.
- [110] Li M, Cheng W, Xie R. Design and experiments of a quasi-zero-stiffness isolator with a noncircular cam-based negative-stiffness mechanism. *J Vib Control* 2020; 26:1935–47.
- [111] Li M, Cheng W, Xie R. A quasi-zero-stiffness vibration isolator using a cam mechanism with user-defined profile. *Int J Mech Sci* 2021;189:105938.
- [112] Zou D, Liu G, Rao Z, et al. A device capable of customizing nonlinear forces for vibration energy harvesting, vibration isolation, and nonlinear energy sink. *Mech Syst Signal Process* 2021;147:107101.
- [113] Yao Y, Li H, Li Y, et al. Analytical and experimental investigation of a high-static-low-dynamic stiffness isolator with cam-roller-spring mechanism. *Int J Mech Sci* 2020;186:105888.
- [114] Zhu G, Cao Q, Wang Z, et al. Road to entire insulation for resonances from a forced mechanical system. *Sci Rep* 2022;12:21167.
- [115] Wang K, Zhou JX, Chang Y, et al. A nonlinear ultra-low-frequency vibration isolator with dual quasi-zero-stiffness mechanism. *Nonlinear Dyn* 2020;101: 755–73.
- [116] Yan G, Zou HX, Wang S, et al. Large stroke quasi-zero stiffness vibration isolator using three-link mechanism. *J Sound Vib* 2020;478:115344.
- [117] Yuan S, Sun Y, Zhao J, et al. A tunable quasi-zero stiffness isolator based on a linear electromagnetic spring. *J Sound Vib* 2020;482:115449.
- [118] Yan G, Wu ZY, Wei XS, et al. Nonlinear compensation method for quasi-zero stiffness vibration isolation. *J Sound Vib* 2022;523:116743.
- [119] Yan G, Qi WH, Shi JW, et al. Bionic paw-inspired structure for vibration isolation with novel nonlinear compensation mechanism. *J Sound Vib* 2022;525:116799.
- [120] Zhao TY, Yan G, Qi WH, et al. Magnetically modulated tetrahedral structure for low frequency vibration isolation with adjustable load capacity. *Int J Mech Sci* 2023;251:108335.
- [121] Abolfathi A, Brennan MJ, Waters TP, et al. On the Effects of Mistuning a Force-Excited System Containing a Quasi-Zero-Stiffness Vibration Isolator. *J Vib Acoust* 2015;137:044502.
- [122] Araki Y, Asai T, Kimura K, et al. Nonlinear vibration isolator with adjustable restoring force. *J Sound Vib* 2013;332:6063–77.
- [123] Ye K, Ji JC, Brown T. Design of a quasi-zero stiffness isolation system for supporting different loads. *J Sound Vib* 2020;471:115198.
- [124] Zheng Y, Shangguan WB, Yin Z, et al. Design and modeling of a quasi-zero stiffness isolator for different loads. *Mech Syst Signal Process* 2023;188:110017.
- [125] Carrella A, Brennan MJ, Waters TP, et al. Force and displacement transmissibility of a nonlinear isolator with high-static-low-dynamic-stiffness. *Int J Mech Sci* 2012;55:22–9.
- [126] Malatkar P, Nayfeh AH. Calculation of the jump frequencies in the response of SDOF non-linear systems. *J Sound Vib* 2002;254:1005–11.
- [127] Hao Z, Cao Q. The isolation characteristics of an archetypal dynamical model with stable-quasi-zero-stiffness. *J Sound Vib* 2015;340:61–79.
- [128] Liu C, Yu K, Liao B, et al. Enhanced vibration isolation performance of quasi-zero-stiffness isolator by introducing tunable nonlinear inerter. *Commun Nonlinear Sci Numer Simul* 2021;95:105654.
- [129] Liu C, Yu K. A high-static-low-dynamic-stiffness vibration isolator with the auxiliary system. *Nonlinear Dyn* 2018;94:1549–67.
- [130] Shin K. On the Performance of a Single Degree-of-Freedom High-Static-Low-Dynamic Stiffness Magnetic Vibration Isolator. *Int J Precis Eng Manuf* 2014;15: 439–45.
- [131] Lu Z, Brennan MJ, Yang T, et al. An investigation of a two-stage nonlinear vibration isolation system. *J Sound Vib* 2013;332:1456–64.
- [132] Wang Y, Li S, Neild SA, et al. Comparison of the dynamic performance of nonlinear one and two degree-of-freedom vibration isolators with quasi-zero stiffness. *Nonlinear Dyn* 2017;88:635–54.
- [133] Wang X, Zhou J, Xu D, et al. Force transmissibility of a two-stage vibration isolation system with quasi-zero stiffness. *Nonlinear Dyn* 2017;87:633–46.
- [134] Lu Z, Yang T, Brennan MJ, et al. Experimental Investigation of a Two-Stage Nonlinear Vibration Isolation System With High-Static-Low-Dynamic Stiffness. *J Appl Mech* 2017;84:021001.
- [135] Wang Q, Zhou J, Wang K, et al. Design and experimental study of a two-stage nonlinear vibration isolators with quasi-zero stiffness. *Commun Nonlinear Sci Numer Simul* 2023;122:107246.
- [136] Deng T, Wen G, Ding H, et al. A bio-inspired isolator based on characteristics of quasi-zero stiffness and bird multi-layer neck. *Mech Syst Signal Process* 2020;145: 106967.
- [137] Liu C, Tang J, Yu K, et al. On the characteristics of a quasi-zero-stiffness vibration isolator with viscoelastic damper. *Appl Math Model* 2020;88:367–81.
- [138] Liu C, Yu K, Tang J. New insights into the damping characteristics of a typical quasi-zero-stiffness vibration isolator. *Int J Non-Linear Mech* 2020;124:103511.
- [139] Shahraeeni M, Sorokin V, Mace B, et al. Effect of damping nonlinearity on the dynamics and performance of a quasi-zero-stiffness vibration isolator. *J Sound Vib* 2022;526:116822.
- [140] Cheng C, Li S, Wang Y, et al. Force and displacement transmissibility of a quasi-zero stiffness vibration isolator with geometric nonlinear damping. *Nonlinear Dyn* 2017;87:2267–79.
- [141] Meng Q, Yang X, Li W, et al. Research and Analysis of Quasi-Zero-Stiffness Isolator with Geometric Nonlinear Damping. *Shock Vib* 2017;2017:6719054.
- [142] Liu Y, Xu L, Song C, et al. Dynamic characteristics of a quasi-zero stiffness vibration isolator with nonlinear stiffness and damping. *Arch Appl Mech* 2019;89: 1743–59.
- [143] Dong G, Zhang Y, Luo Y, et al. Enhanced isolation performance of a high-static-low-dynamic stiffness isolator with geometric nonlinear damping. *Nonlinear Dyn* 2018;93:2339–56.
- [144] Hao Z, Cao Q, Wiercigroch M. Two-sided damping constraint control strategy for high-performance vibration isolation and end-stop impact protection. *Nonlinear Dyn* 2016;86:2129–44.
- [145] Ho C, Lang ZQ, Billings SA. Design of vibration isolators by exploiting the beneficial effects of stiffness and damping nonlinearities. *J Sound Vib* 2014;333: 2489–504.
- [146] Milovanovic Z, Kovacic I, Brennan MJ. On the Displacement Transmissibility of a Base Excited Viscously Damped Nonlinear Vibration Isolator. *J Vib Acoust* 2009; 131:054502.
- [147] Wen G, Lin Y, He J. A quasi-zero-stiffness isolator with a shear-thinning viscous damper. *Appl Math Mech (Engl Ed)* 2022;43:311–26.
- [148] Liu X, Zhao Q, Zhang Z, et al. An experiment investigation on the effect of Coulomb friction on the displacement transmissibility of a quasi-zero stiffness isolator. *J Mech Sci Technol* 2019;33:121–7.
- [149] Donmez A, Cigeroglu E, Ozgen GO. An improved quasi-zero stiffness vibration isolation system utilizing dry friction damping. *Nonlinear Dyn* 2020;101:107–21.
- [150] Hu X, Zhou C. Dynamic analysis and experiment of Quasi-zero-stiffness system with nonlinear hysteretic damping. *Nonlinear Dyn* 2022;107:2153–75.

- [151] Yan B, Wang X, Ma H, et al. Hybrid Time-Delayed Feedforward and Feedback Control of Lever-Type Quasi-Zero-Stiffness Vibration Isolators. *IEEE Trans Ind Electron* 2024;71:2810–9.
- [152] Sun X, Xu J, Jing X, et al. Beneficial performance of a quasi-zero-stiffness vibration isolator with time-delayed active control. *Int J Mech Sci* 2014;82:32–40.
- [153] Xu J, Sun X. A multi-directional vibration isolator based on Quasi-Zero-Stiffness structure and time-delayed active control. *Int J Mech Sci* 2015;100:126–35.
- [154] Li Y, Xu D. Chaotification of quasi-zero-stiffness system with time delay control. *Nonlinear Dyn* 2016;86:353–68.
- [155] Cheng C, Hu Y, Ma R, et al. Beneficial performance of a quasi-zero-stiffness vibration isolator with displacement-velocity feedback control. *Nonlinear Dyn* 2023;111:5165–77.
- [156] Ma Z, Zhou R, Yang Q, et al. A semi-active electromagnetic quasi-zero-stiffness vibration isolator. *Int J Mech Sci* 2023;252:108357.
- [157] Chang Y, Zhou J, Wang K, et al. Theoretical and experimental investigations on semi-active quasi-zero-stiffness dynamic vibration absorber. *Int J Mech Sci* 2022;214:106892.
- [158] Liu S, Feng L, Zhao D, et al. A real-time controllable electromagnetic vibration isolator based on magnetorheological elastomer with quasi-zero stiffness characteristic. *Smart Mater Struct* 2019;28:085037.
- [159] Wen G, He J, Liu J, et al. Design, analysis and semi-active control of a quasi-zero stiffness vibration isolation system with six oblique springs. *Nonlinear Dyn* 2021;106:309–21.
- [160] Le TD, Ahn KK. A vibration isolation system in low frequency excitation region using negative stiffness structure for vehicle seat. *J Sound Vib* 2011;330:6311–35.
- [161] Le TD, Ahn KK. Active pneumatic vibration isolation system using negative stiffness structures for a vehicle seat. *J Sound Vib* 2014;333:1245–68.
- [162] Liao X, Zhang N, Du X, et al. Theoretical Modeling and Vibration Isolation Performance Analysis of a Seat Suspension System Based on a Negative Stiffness Structure. *Appl Sci* 2021;11:6928.
- [163] Wang Y, Li S, Cheng C, et al. Adaptive control of a vehicle-seat-human coupled model using quasi-zero-stiffness vibration isolator as seat suspension. *J Mech Sci Technol* 2018;32:2973–85.
- [164] Chen Z, Yu S, Wang B, et al. The research about application of quasi-zero stiffness vibration isolation technology in a large vehicle-mounted optic-electronic equipment. *Ain Shams Eng J* 2023;14:101841.
- [165] Xu X, Jiang X, Chen L, et al. Semi-active control of a new quasi-zero stiffness air suspension for commercial vehicles based on event-triggered H_∞ dynamic output feedback. *Nonlinear Dyn* 2023.
- [166] Boua HB, Nbendjo BRN, Woaf P. Isolation performance of a quasi-zero stiffness isolator in vibration isolation of a multi-span continuous beam bridge under pier base vibrating excitation. *Nonlinear Dyn* 2020;100:1125–41.
- [167] Boua HB, Nbendjo BRN. Analysis of the Performance of Quasi-zero Stiffness Isolator on the Reduction of Vibration on a Multi-span Continuous Beam Bridge Under Moving Mass. *J Vib Eng Technol* 2022.
- [168] Attary N, Symans M, Nagarajaiah S, et al. Numerical simulations of a highway bridge structure employing passive negative stiffness device for seismic protection. *Earthq Eng Struct Dyn* 2015;44:973–95.
- [169] Attary N, Symans M, Nagarajaiah S, et al. Performance Evaluation of Negative Stiffness Devices for Seismic Response Control of Bridge Structures via Experimental Shake Table Tests. *J Earthq Eng* 2015;19:249–76.
- [170] Zhu G, Liu J, Cao Q, et al. A two degree of freedom stable quasi-zero stiffness prototype and its applications in aseismic engineering. *Sci China Technol Sci* 2020;63:496–505.
- [171] Valeev A, Tokarev A, Zотов A. Material with Quasi-Zero Stiffness for Vibration Isolation in Civil and Industrial Structures and Buildings. *IOP Conf Ser: Earth Environ Sci* 2019;272:032048.
- [172] Liu D, Liu Y, Sheng D, et al. Seismic Response Analysis of an Isolated Structure with QZS under Near-Fault Vertical Earthquakes. *Shock Vib* 2018;2018:9149721.
- [173] Eskandary-Malayeri F, Ilanko S, Mace B, et al. Experimental and numerical investigation of a vertical vibration isolator for seismic applications. *Nonlinear Dyn* 2022;109:303–22.
- [174] Li H, Askari M, Li J, et al. A novel structural seismic protection system with negative stiffness and controllable damping. *Struct Control Health Monit* 2021;28:e2810.
- [175] Cimellaro GP, Domianeschi M, Warn G. Three-Dimensional Base Isolation Using Vertical Negative Stiffness Devices. *J Earthq Eng* 2020;24:2004–32.
- [176] Zhou Y, Chen P, Mosqueda G. Analytical and Numerical Investigation of Quasi-Zero Stiffness Vertical Isolation System. *J Eng Mech* 2019;145:04019035.
- [177] Zhou Y, Chen P, Mosqueda G. Numerical Studies of Three-Dimensional Isolated Structures with Vertical Quasi-Zero Stiffness Property. *J Earthq Eng* 2022;26:3601–22.
- [178] Ding H, Ji J, Chen LQ. Nonlinear vibration isolation for fluid-conveying pipes using quasi-zero stiffness characteristics. *Mech Syst Signal Process* 2019;121:675–88.
- [179] Wang Q, Zhou J, Xu D, et al. Design and experimental investigation of ultra-low frequency vibration isolation during neonatal transport. *Mech Syst Signal Process* 2020;139:106633.
- [180] Zhou J, Wang K, Xu D, et al. Vibration isolation in neonatal transport by using a quasi-zero-stiffness isolator. *J Vib Control* 2018;24:3278–91.
- [181] Jing X, Zhang L, Feng X, et al. A novel bio-inspired anti-vibration structure for operating hand-held jackhammers. *Mech Syst Signal Process* 2019;118:317–39.